Selective packaging of pathogenic non-coding RNAs into plant exosomes mediated through Phloem Protein 2 and Tetraspanin 8 may represent a key mechanism for their cross-kingdom transmission

Neha Devi[1], Nisha Devi[1], Vasudha Sharma[1], Ravi Gupta[2], Sunny Dhir[1]*, Yashika Walia[1]*

[1]Molecular Plant Virology Group, R&D Lab, Department of Bio-Sciences & Technology, Maharishi Markandeshwar (Deemed to be University), Mullana, Ambala-133207 HR India

[2]Plant Stress Physiology and Proteomics Laboratory, College of General Education, Kookmin University, Seoul, South Korea

Neha Devi: nehadevi611999@gmail.com

Vasudha Sharma: vasu.3096sharma@gmail.com

Nisha Devi: nishapahal99@gmail.com

*Corresponding Authors

Dr. Yashika Walia; yashikawalia@gmail.com, yashika.dhir@mmumullana.org

ORCID ID: 0000-0002-0796-0050

Dr. Sunny Dhir; sunny72155@gmail.com, sunny.dhir@mmumullana.org

ORCID ID: 0000-0002-3790-8333

Abstract

The plant apoplast and extracellular vesicles (EVs) contain diverse RNA species, including small RNAs, long non-coding RNAs, and circular RNAs, many of which cross kingdom boundaries through EV-mediated transport. Viroid RNAs—pathogenic circular non-coding RNAs—are known to move from plants to fungi and insects, though the mechanism remains unclear. Using apple scar skin viroid (ASSVd) and cucumber as a host, we demonstrate that viroid RNAs in circular, linear, and small RNA forms are present in cucumber EVs. ASSVd RNA exhibits features of extracellular RNAs, such as m6A methylation and five EXOmotifs. Through mass spectrometry and immunoblotting, we identify tetraspanin 8 (CsTET8) as a conserved EV marker and report CsPP2, a phloem lectin with an RNA-binding domain, as a novel EV-associated protein. RNA co-immunoprecipitation and immuno-enrichment assays reveal that CsPP2 and ASSVd co-localize in CsTET8-positive EVs, with direct interactions between CsPP2-CsTET8 and CsPP2-ASSVd. We propose CsPP2 functions as an RNA-sorting protein that mediates RNA loading into EVs. Further, we show that whiteflies can acquire ASSVd via EVs and transmit it to healthy plants, indicating a cross-kingdom transmission route. These findings establish viroid RNAs as a model system to study the molecular basis of RNA trafficking across biological kingdoms.

Keywords: Extracellular vesicles, Viroid RNA, Phloem Protein 2, Tetraspanin 8, Exomotifs, m6A methylation

Introduction

The role of the apoplast and EVs in mediating cross-kingdom RNA trafficking has gained attention recently (Zhang et al., 2016, Wang et al., 2024). EVs are small, membrane-bound vesicles secreted by cells that can encapsulate a variety of biomolecules, including RNA (Zhang et al., 2016; He et al., 2021, Karimi et al., 2022; Wang et al., 2024). Plants are known to contain three classes of EVs (Ambrosonethe et al., 2023). The first class is represented by exosomes with sizes ranging from 30-150nm which are specifically enriched in tetraspanin 8 (TET8), an ortholog of mammalian CD63, CD81, and CD151 (Chen et al., 2022, Jankovičová et al., 2020). The second class is represented by micro-vesicles with sizes ranging from 150-300nm and are associated with syntaxins proteins, of which Penetration 1 (PEN1) is well characterized (Rutter et al., 2017). The third class is represented by EXPO vesicles which are double membrane bodies fused with the plasma membrane (PM), releasing a single membrane vesicle into the cell wall (Wang et al., 2010). Exo70E2 is essential for exocyst subunit recruitment and EXPO formation in both plants and animals (Ding et al., 2014).

Plant apoplast and EVs are enriched in various RNA species, such as long non-coding RNAs (lncRNA), circular RNAs, (circRNA) micro RNAs (miRNAs), and tasiRNAs (Karimi et al., 2022). The process of cross-kingdom RNA transfer via EVs was first observed during the interaction between Arabidopsis and *Botrytis cinerea*, where pathogen-derived small RNAs (sRNAs) were shown to travel across kingdoms and interact with plant argonaute (AGO) to target mitogen-activated protein kinase transcripts, promoting pathogen colonization (Weiberg et al., 2013). Subsequent studies revealed that plants can send their small RNAs in TET8-specific exosomes to suppress fungal virulence genes (Cai et al., 2018). In addition, they also carry mRNAs that are translated into fungi and reduce their pathogenicity (Wang et al., 2024). Recent studies have identified various mechanisms involved in the loading of RNA into EVs. Specifically, RNA-binding proteins such as AGO1, annexins, and RNA helicases play significant roles in the incorporation of plant small RNAs into TET8-specific exosomes (He et al., 2021; Karimi et al., 2022). Furthermore, glycine-rich binding protein (GRP7) and AGO2 have been linked to the secretion of N6-methyladenosine (m6A) modified circular and long non-coding RNAs, as well as small RNAs in the apoplast (Karimi et al., 2022). Similar to the animals, circular RNAs in the plant apoplast are notably enriched with m6A modifications (Sabrina Garbo

et al., 2024; Karimi et al., 2022). Certain factors have been identified in animals and plants that could assist the sorting of RNAs inside the vesicles. These factors encompass characteristics such as a high GC content, the presence of an EXOmotif (a motif known to facilitate preferential sorting of RNA into exosomes or EVs), and their ability to modify RNAs and interact with RNA binding proteins (O'Grady et al., 2022, Ruben Garcia-Martin et al., 2022, Sabrina Garbo et al., 2024, Xiao-Man Liu 2025).

A class of non-coding circular RNAs is represented by viroids which are RNA-only pathogens infecting plants with distinct structural and functional properties (Flores et al., 2016; Navarro et al., 2021; Hammond, 2017). Despite their small size (246-401nts) and non-coding properties, they autonomously replicate within infected plant cells and cause a variety of diseases. The ability of viroids to infect plants is enabled by their secondary structure (Branch et al., 1984; Daros et al., 1994; Warrilow et al., 1999; Navarro et al., 2000; Rodio et al., 2007), which is crucial for their replication and movement and allows hijacking of plant cellular machinery for their propagation (Schnölzer et al., 1985; Schmitz and Riesner, 1998; Sano et al., 1992; Reanwarakorn & Semancik, 1998). Recent studies have shown that viroids are not limited to infecting plants but can also affect other biological kingdoms, including fungi, insects, and bacteria (Tian et al., 2020; Walia et al., 2015; Leichtfried et al., 2022; Afanasenko et al., 2022). This cross-kingdom infection potential suggests that viroids, much like other RNA entities, can traverse biological barriers and may play a role in complex ecological interactions (Cai et al., 2019, Wang et al., 2024). For example, research on apple scar skin viroid (ASSVd) demonstrated that viroids get transmitted from infected apple trees to fungi, such as *Alternaria alternata*, a common plant pathogen (Tian et al., 2022). We have previously reported that the glass-house whitefly, *Trialeurodes vaporariorum*, mediates the transmission of ASSVd and cucumber PP2 assists in its acquisition and transmission (Walia et al., 2015). Moreover, certain aphid species and codling moth larvae, which feed directly on infected apple trees, were found to transmit apple chlorotic fruit spot viroid (ACFSVd), highlighting the role of insect vectors in cross-kingdom viroid transmission (Leichtfried et al., 2022). Potato spindle tuber viroid (PSTVd) transmission from infected plants to *Phytophthora infestans* also emphasizes the inter-kingdom dynamics of viroid spread (Afanasenko et al., 2022).

104 All these findings together suggest that viroids, as circular non-coding RNAs, may take
105 advantage of RNA sorting and encapsulation mechanisms within EVs to facilitate their
106 intercellular movement and potential cross-kingdom dissemination. By associating with EVs,
107 viroids could bypass the hostile intracellular environment of the host, enabling long-distance
108 transport or transmission across different organisms. Using ASSVd as a model for circular non-
109 coding RNAs and cucumber as its host, we demonstrate that viroid RNAs in various forms are
110 present in cucumber EVs. ASSVd RNA exhibits extracellular RNA signatures, such as m6A
111 methylation and EXOmotifs, which may facilitate EV packaging. Protein identification by mass
112 spectrometry (MS) identifies TET8 as a conserved EV marker and PP2, a phloem lectin with an
113 RNA-binding domain, as a novel E-associated protein. We demonstrate the interaction between
114 ASSVd-PP2-TET8 and speculate that PP2 might assist in RNA loading inside EVs. Lastly, we
115 show that whiteflies can acquire and transmit viroid RNAs via EVs, highlighting a potential
116 cross-kingdom RNA trafficking mechanism.

117 **Material and Methods**

118 **Plant Growth**

119 *Cucumis sativus* (Var. Summer Green) and *Nicotiana benthamiana* seeds were cultivated in pots
120 containing a mixture of cocopeat, compost, and vermiculite/Perlite in a 1:1:1 ratio. The plants
121 were kept in an insect-proof plant growth chamber equipped with fluorescent tubes under
122 controlled conditions with a temperature of 24±2°C, relative humidity of 70-80%, and a 12-hour
123 light/12-hour dark cycle.

124 ***In vitro* synthesis of dimeric ASSVd (+) RNA and transcript inoculation**

125 To generate positive-sense RNA transcripts of ASSVd, recombinant plasmids containing the
126 dimeric ASSVd insert in the correct positive orientation within the pGEMT-easy vector were
127 linearized using *Spe*I. In vitro transcription was carried out using the T7 Highscribe Kit (NEB,
128 USA) according to the manufacturer's protocol. Approximately 100 ng of the RNA transcripts
129 were subsequently used to infect the first true leaf of cucumber plants through mechanical
130 inoculation using carborundum-dust. The water-inoculated plants were used as controls in all
131 experiments.

132 **RNA extraction and RT-PCR for ASSVd detection**

133 Total RNA was extracted from 100 mg of cucumber leaves using the RNAiso plus (TakaraBio,
134 USA; Walia et al., 2020). Briefly, 100mg of the cucumber leaves (viroid infected and mock)
135 were frozen in liquid nitrogen, ground in Trizol buffer, and incubated with chloroform. After
136 centrifugation, the supernatant was mixed with isopropanol for RNA precipitation and stored at -
137 20°C. The RNA pellet was then washed with 75% ethanol and eluted in 20 µL of nuclease-free
138 water. The RNA was quantified using Quantus™ Fluorometer (Promega) and 1µg of RNA was
139 used for RT-PCR with viroid-specific primers ASSVdICc and ASSVdICh (Table S1) (Walia et
140 al., 2014). Reverse transcription was performed using verso cDNA synthesis kit (Thermo
141 Scientific, USA) at 42°C for 60 minutes, followed by PCR using Phusion DNA polymerase
142 (Thermo Scientific, USA) under specified cycling conditions for ASSVd detection (Walia et al.,
143 2014). The PCR products were analyzed on 1.5% agarose gel electrophoresis.

144 **Isolation of AWF**

145 Apoplastic washing fluid (AWF) from cucumber leaves was isolated as described previously
146 (O'Leary et al., 2014). The leaf petioles were excised, followed by washing and drying the leaves
147 (Fig. S1). The leaves were placed in a 60 mL syringe filled with an infiltration buffer (20mM
148 MES, 2mM $CaCl_2$, 0.1M NaCl, pH 6.0). Carefully without damaging the leaves, a negative
149 pressure was created by pulling the plunger gently until the leaves turned dark green. The leaves
150 were removed and dried and 3-4 leaves rolled were placed in a 12 mL syringe inside a 50 mL
151 falcon tube. The tube was wrapped with parafilm and centrifuged at 4,000 rpm for 30 minutes to
152 collect the AWF.

153 **Trypan blue staining of leaves after AWF isolation for cell death analysis**

154 The integrity of the isolated AWF was confirmed by cell death assay by staining the leaves in
155 trypan blue solution using the protocol as described (http://resources.rothamsted.ac.uk).

156 **RNA isolation and RT-PCR detection of ASSVd from AWF**

157 One ml of isolated AWF was concentrated to 100µl using an Amicon® Ultra Centrifugal Filter,
158 10 kDa MWCO (Millipore, USA). RNA was isolated using RNAiso plus (Takara Bio, USA).
159 Briefly, 1ml of RNAiso plus was added to 100µl of AWF followed by the addition of the
160 chloroform. The RNA was precipitated using isopropanol and suspended in 30µl of RNase-free
161 water. One microgram of RNA was used for RT-PCR as mentioned earlier.

162 **Isolation of EVs**

163 Pure-EVs SEC columns were used to isolate EVs from cucumber plants (mock/viroid infected).
164 For EV isolation, 20 mL of isolated AWF was concentrated to 2 mL using an Amicon filter unit
165 (10kDa cutoff) (Millipore, USA) and was subjected to Pure-EVs SEC columns (Hansa Biomed
166 Life Sciences, Estonia) according to the manufacturer's instructions. Briefly, the column was
167 washed with 3 volumes of 1× PBS buffer to remove preservative buffer residues. The sample
168 containing EVs (up to 2 mL) was then loaded into the column and eluted with 1× PBS buffer as
169 the mobile phase. Fractions collected were labeled 1-7 as void volume, 8-13 as the EV fraction,
170 and 14-23 as the protein sample (Fig. S2).

171 **Dynamic Light Scattering (DLS) analyses of EVs**

172 The DLS analyses were performed in a Litesizer 500 (Anton Paar, Germany). 10 µL of isolated
173 EVs were suspended in 990 µL of 1× sterile PBS buffer, loaded into a disposable cuvette, and
174 placed in the litesizer 500. For reproducibility, and standardization, the parameter values were
175 fixed as follows; Temp-25°C, equilibration time-30s, processed runs-5, and Time for each run
176 10s. The size or homogeneity of exosomes was recognized through the radius or the % Intensity,
177 respectively.

178 **Transmission electron microscopy of EVs**

179 Purified EVs (10 µl) were diluted with an equal volume of 4% paraformaldehyde at 4°C for 30
180 min, and then carefully placed on a carbon-coated 300-mesh copper grid for 20 min, followed by
181 fixed by 1% glutaraldehyde for 5 min. After two washings, the grids were contrasted with 2%
182 uranyl acetate and then washed again two times. The morphology of isolated exosomes was
183 visualized with TEM (MAKE: JEOL MODEL: JEM 2100 plus).

184 **Trypsin, RNase treatment, RNA isolation, and RT-PCR from EVs**

185 To determine whether the viroid RNA was present inside or outside EVs, RNase protection
186 assays were performed. Briefly, 100µl of Purified EVs were treated with 25 µg/µL trypsin
187 (Sigma Life Sciences, USA). Samples were incubated at 37°C for 16-18 hours, followed by the
188 addition of 1U of Proteinase K (Invitrogen, USA)/1mM of PMSF (Sigma, USA) to inactivate
189 trypsin. For isolating the RNA from the EV surface the above EV samples were precipitated with

190 3 volume ethanol and 1/10 sodium acetate overnight followed by isolation of RNA with RNAiso
191 plus next day. For isolating the RNA inside EVs the purified EVs (100µL) were treated with
192 trypsin + trypsin inhibitor + RNaseA + RNase inhibitor to degrade the outside RNA followed by
193 treatment with 1% (v/v) Triton X-100 (Himedia) to rupture the EVs. RNA isolation using
194 RNAiso plus was carried out to isolate the RNA inside EVs. The isolated RNA was quantified
195 and 200ng of the total RNA was used for RT-PCR from the detection of ASSVd from EV^O and
196 EV^I as described above. The concentration of trypsin and RNase used in the assays was
197 standardized by taking different dilutions of trypsin and RNase for protein degradation and RNA
198 degradation, respectively (Fig. S3 and S4).

199 **Urea PAGE and Northern Blot for ASSVd detection**

200 Viroid-infected samples from total leaf, AWF, and EVs (EV^O and EV^I) along with mock RNA
201 from leaf were analyzed using Denaturing Polyacrylamide gel electrophoresis (15%
202 polyacrylamide and 7M Urea). The RNA samples (3µg for AWF, EV^O, EV^I 10ug, and 3ug for
203 CL from infected and 3ug from Mock) were denatured at 65°C in 2x RNA dye (Thermo
204 Scientific, USA) for 10 minutes and were separated in 0.5× TBE buffer for 2h at 90V. The total
205 RNAs were visualized by staining with Diamond Nucleic acid stain (Promega) and then
206 transferred onto a nylon membrane using 1× TBE transfer buffer. The RNAs were cross-linked
207 on a nylon membrane in a UV crosslinker followed by pre-hybridization at 65°C for 3hrs. The
208 membrane was incubated overnight at 65°C in hybridization buffer with gentle shaking along
209 with a 3' labeled biotin probe. The membrane was rinsed with washing buffer (1× SSC. 0.1%
210 SDS) thrice for 10 minutes at room temperature and blocked in a blocking buffer (0.1% Malic
211 acid buffer (Roche). The membrane was incubated with HRP-conjugated anti-streptavidin
212 antibody (Sigma, USA) at 1:5000 dilutions for 1h. After a final wash in maleic acid and 0.3%
213 Tween-20 containing buffer, the blot was visualized using ChemiDoc (Protein Simple, Biotechne,
214 USA).

215 **Generation of negative sense 3'-biotin labeled ASSVd probe**

216 A 3'-biotin-labeled RNA probe was prepared and used for viroid detection using northern
217 hybridization. For probe synthesis, a PCR was carried out using ASSVd plasmid as a template
218 and primers FP1 and RP4 to generate negative sense viroid amplicon along with the T7 promoter
219 sequence. The desired amplicon of 330bp was cut and eluted. Two micrograms of gel eluted

220 product was directly used to generate RNA transcript using a T7 in vitro RNA transcription kit
221 (Thermo Scientific, USA). The transcript at the 3' end was ligated to pcp-biotin (Jena
222 Biosciences) using T4 RNA Ligase (Promega, USA). The reaction was kept at 16ºC overnight.
223 The labeled transcript was purified using a Monarch RNA cleanup column (New England
224 Biolabs, USA) and was used for hybridization at a concentration of 100ng/10ml of hybridization
225 buffer (Fig. S5).

226 **Immunoprecipitation with m6A antibody**

227 Total RNA was isolated from apoplastic fluid, and EVs using RNAisol plus as described earlier
228 and quantified using a Quantus fluorimeter (Promega, USA). For AWF and EVs, 5µg RNA was
229 incubated with an m6A antibody (Epigenetek-A-1801-020) in IP buffer (50mM Tris HCl pH 7.5,
230 150mM NaCl, 0.5% NP-40) at 4°C for 4-5 hours, followed by the addition of Protein A/G
231 agarose beads (Merck, USA) and incubated overnight. The samples were washed with IP buffer
232 and eluted from beads using RNAiso plus. The isolated RNA was suspended in 100µl of RNase-
233 free water. For spotting on the membrane, 10µl of the RNA was denatured at 65°C for 10
234 minutes and applied to a nylon membrane (for detecting with ASSVd probe) and cross-linked.
235 The membrane was pre-hybridized, incubated overnight with a negative sense ASSVd-specific
236 biotin probe, washed, and blocked. After incubation with HRP-labelled streptavidin (Sigma,
237 USA), m6A-modified RNA was visualized using a ChemiDoc system (Protein Simple,
238 Biotechne, USA). For detecting with anti m6A antibody the RNA was spotted on the
239 nitrocellulose membrane and the membrane was blocked in 5% skim milk solution with
240 overnight incubation with 1:5000 dilution of anti m6A antibody (Epigenetek-A-1801-020). The
241 next day membranes were washed and incubated with goat anti-rabbit HRP-conjugated
242 secondary antibodies, washed and visualized using ECL substrate (Biorad, USA), and imaged
243 with a ChemiDoc system (Protein Simple, Biotechne, USA) or X-ray film.

244 **Mass spectrometry**

245 EVs fraction (100µl) was treated with trypsin followed by incubation with trypsin inhibitor and
246 were then treated with 0.1% Triton X-100. The proteins were TCA precipitated and partially
247 resolved by polyacrylamide gel electrophoresis till they entered the resolving gel. The region was
248 excised and sequenced using HR-LCMS, SAIF facility at IIT-BOMBAY. Briefly, the gel slices
249 were subjected to in-gel trypsin digestion followed by desalting and subjected to LC/MS/MS

250 analysis in Q-Exactive Plus Orbitrap high-resolution MS (Thermo Scientific). The MS spectra
251 were acquired at a resolution of 70,000 in a mass range of 350-2500 m/z. Eluted samples were
252 used for MS/MS events (resolution of 17,500), measured in a data-dependent mode for the 15
253 most abundant peaks (Top15 method).

254 **Protein identification and GO enrichment tools**

255 The raw MS/MS spectra were analyzed using the software Thermo Proteome Discoverer 2.2
256 against the Arabidopsis (TAIR) and cucumber database (Cucurbit genomics-
257 http://cucurbitgenomics.org/). The ShinyGO v0.82 (ShinyGO 0.82 (sdstate.edu)) and string tools
258 were used (STRING: functional protein association networks (string-db.org) for GO analyses.
259 Venn diagram was constructed using the software Bioinformatics & Evolutionary Genomics
260 (Draw Venn Diagram (ugent.be).

261 **Immunoblots**

262 For immunoblots, cell lysate was prepared by grinding 50mg of leaf tissue in 500ụl of protein
263 extraction buffer (50mM Tris HCl pH 7.5, 150mM NaCl, 10mM $MgCl_2$, 2.5mM EDTA, 1mM
264 DTT, 10% Glycerol, 1x protease inhibitor, 1mM PMSF). 20ụl of cell lysate, concentrated AWF,
265 and EVs (EVO and EVI) were mixed with 3 µL of 6× SDS loading buffer, heated at 99°C for 10
266 minutes, and loaded onto a 15% PAGE, and after run proteins were transferred to a nitrocellulose
267 membrane (for dot blots, the dots were applied on the nitrocellulose membrane directly without
268 the SDS dye). Membranes were blocked with 5% skim milk in TBST and incubated overnight at
269 4°C with primary antibodies (1:1000 for TET8 (PhytoAb-PHY2750A), 1:10000 for CsPP2
270 (Walia et al., 2015, 1:10000 anti-GFP (BioBharati Life Science, India) and 1:3000 anti-HA
271 (BioBharati, Life Science, India), anti-actin (Sigma) mouse monoclonal 1:20000 dilution.
272 Membranes were washed and incubated with 1:10000 goat anti-rabbit/anti-mouse HRP-
273 conjugated secondary antibodies (BioBharati, Life Science, India). After a final wash, proteins
274 were visualized using the ECL substrate (Biorad, USA) and imaged with a ChemiDoc system
275 (Protein Simple, Biotechne, USA) or X-ray film.

276 **RNA immunoprecipitation assay (RIP assay)**

277 For RNA immunoprecipitation from the leaf, 1g/ml of viroid-infected leaf tissue was ground in
278 protein extraction buffer supplemented with RNase inhibitor, and 500µl of lysate was used for

279 RNA immunoprecipitation assay. For RNA immunoprecipitation from infected AWF, 5ml of
280 AWF isolated from viroid-infected leaves was concentrated to 500µl solution using an Amicon
281 filter. Both the lysate and AWF were incubated with 5mg of CsPP2 antibody for 4h at 4°C with
282 rotation followed by the addition of protein A/G agarose beads overnight. The next day the beads
283 were pelleted with centrifugation at 3000 rpm for 5 minutes and washed three times with protein
284 extraction buffer supplemented with RNase inhibitor. The beads were eluted in 100ul of RNAse-
285 free water. Half of the beads were heated at 100°C for 10 minutes to release bead-bound proteins
286 for subsequent immunoblot. The rest of the beads were proceeded for RNA isolation using
287 RNAiso plus. The RNA was quantified and used for the detection of ASSVd by RT-PCR or
288 loaded on 15% denaturing PAGE to visualize the total immunoprecipitated RNAs using
289 Diamond Nucleic acid stain (Promega) as described earlier.

290 **Immunoenrichment of TET8 exosomes**

291 The isolated intact EVs were treated with trypsin overnight, followed by the addition of a trypsin
292 inhibitor. Next, RNase was added for one hour, and then RNase inhibitor was used to inactivate
293 the RNase. The intact EVs were incubated with anti-AtTET8 antibody in IP buffer without NP-
294 40 for 4 hours at 4°C with rotation, followed by the addition of protein A/G agarose beads
295 overnight. The next day, the beads were pelleted and washed with IP buffer containing 1%Triton
296 X-100 and RNase inhibitor. The beads were then eluted in RNase-free water, with part of the
297 eluate used for RNA isolation as previously described. The isolated RNA was tested for the
298 presence of ASSVd by RT-PCR, as described earlier. The remaining beads were heated and
299 loaded onto an SDS-PAGE gel for immunoblotting with anti-AtTET8 and anti-CsPP2 antibodies.

300 **Co-Immunoprecipitation assay:** For co-immunoprecipitation assays involving GFP-TET8 and
301 HA-PP2, Nicotiana benthamiana leaves were harvested 48 hours post agroinfiltration. Tissue
302 extracts were homogenized in Protein extraction buffer (PEB) [5 mM Tris-HCl (pH 7.5), 150
303 mM NaCl, 10 mM $MgCl_2$, 1 mM EDTA, 1% NP-40, and 1X protease inhibitor cocktail (Sigma-
304 Aldrich, USA)]. After centrifugation to remove cell debris, the supernatant was pre-cleared using
305 IgG agarose beads (Biobharti Life Sciences, India) for 1 hour at 4°C with rotation. The mixture
306 was centrifuged again, and the IgG agarose bead pellet, used as a non-specific binding control,
307 was collected. The resulting supernatant was incubated overnight at 4°C with anti-GFP agarose
308 beads (BioBharati Life Sciences, India). Following centrifugation, the beads were washed three

309 times with PEB buffer, resuspended in 1× SDS loading dye, and prepared for immunoblot
310 analysis.

311 **Subcellular Localization and Bi-molecular Fluorescence Complementation (BiFC) Assays**

312 *Agrobacterium tumefaciens* strain GV3101 harboring CsTET8 fused to GFP in the binary vector
313 pSITE2CA was infiltrated into mature *N. benthamiana* leaves. At 48 hours post-infiltration (hpi),
314 tissue sections from infiltrated areas were examined using a confocal microscope (NIKON, AIR
315 PLUS). Images were captured using both bright-field and YFP filter settings. For BiFC assays,
316 GV3101 strains carrying CsTET8 and CsPP2 in BiFC-compatible binary vectors (nVENUS and
317 cCFP) were co-infiltrated into *N. benthamiana* leaves in the indicated combinations. Leaf
318 sections were observed under a confocal microscope at 48 hpi. Images were captured using both
319 bright-field and YFP filter settings.

320 **Dynamics of CsTET8 and CsPP2 upon viroid infection**

321 Three cucumber plants were infected with ASSVd transcripts along with mock as control. The
322 samples were harvested at 7dpi, 14dpi, 21dpi and 28dpi. The lysates were prepared in 8M urea,
323 mixed with SDS dye, heated, and loaded on 15% PAGE. The proteins were transferred to the
324 membrane and immunoblotted with CsPP2 and AtTET8 antibodies as described earlier.

325 **Bioinformatic analysis of the ASSVd-CsPP2-CsTE8 interactions**

326 The amino acid sequences of the proteins were obtained from the following accession numbers
327 in GenBank: Tetraspanin-8 (TET8) *Cucumis sativus* Accession XP_004151158.1, Lectin
328 (phloem protein 2) *Cucumis sativus* Accession NP_001292700.1, and ASSVd RNA sequence
329 was of an isolate from Solan with Accession FM178284. The models were generated from the
330 above-mentioned sequences by the Alphafold2 algorithm (Jumper et al., 2021). The quality was
331 assessed using pLDDT scores. The models were visualized using ChimeraX software v 1.7.1
332 (Meng et al., 2023). The interactions of PP2 with TET8 and trimeric interaction of PP2 and
333 TET8 with viroid RNA was studied using AlphaFold3 (Abramson et al., 2024;
334 https://alphafoldserver.com/fold/20a59528fa980c38) that allows structural modeling and
335 interactions of protein and RNA. The quality was assessed using pTM scores. The models were
336 visualized using ChimeraX software v. 1.7.1 (Meng et al., 2023).

337 **Densitometric analysis**- Densitometry was carried out using freely available ImageJ software
338 (https://ImageJ.net/ij/)

339 **EV acquisition and viroid transmission assay**

340 The whiteflies used for the experiment were glasshouse whiteflies (*Trialeurodos vaprorarium*)
341 (Walia et al., 2015) that were maintained on healthy cucumber and tomato plants in an insect-
342 proof cage. For ASSVd acquisition by whiteflies, ten whiteflies were fed each with AWF
343 (depleted of EVs) and EV (depleted of outside RNAs) and water as control. The whiteflies were
344 trapped in 50ml falcon tubes with their top covered with stretched parafilm. The AWF, EV, and
345 water were placed on the parafilm along with food color (turmeric) and covered with a coverslip
346 (Walia et al., 2015). The tubes were kept in a growth rack under 14h light and 10h dark period
347 for 48h and the whiteflies were allowed to feed on the solution. After 48h the five whiteflies
348 were killed using the cold shock method and RNA isolation and RT-PCR for ASSVd detection
349 was done as described earlier. The remaining five whiteflies were made to feed on healthy
350 cucumber plants (five plants) in an insect-proof rack. The whitefly-fed plants were pooled P1
351 (1+2) and P2 (3+4+5) checked for the viroid presence using RT-PCR method with ASSVd-
352 specific primers as described above.

353 For transmission assay using viroid-infected EVs and AWF, three cucumber plants each with
354 AWF (depleted of EVs) and EV (depleted of outside RNAs) were sap inoculated along with leaf
355 sap as positive control and water as negative control. The plants were pooled for individual
356 treatment and checked for the ASSVd presence at 14dpi by RT-PCR method as described earlier.

357 Statistical analysis. All data presented here are representative of at least three biological and
358 technical replicates for each. Statistical analysis details are mentioned in the respective figure
359 legends.

360 **Results**

361 **ASSVd RNA localizes in the apoplast and EVs of cucumber plants**

362 To investigate the presence of viroid RNA in apoplast and EVs, we used cucumber plants
363 infected with dimeric infectious transcripts of ASSVd (Walia et al., 2014). The apoplastic wash
364 fluid (AWF) was isolated from viroid-infected plants, 3-week post ASSVd inoculation, using an

365 infiltration centrifugation method (Fig. S1; O'Leary et al., 2014). SDS-PAGE analysis of the
366 isolated apoplastic proteins showed the absence of the large subunit of RuBisCO (approximately
367 55 kDa), indicating that the AWF was free from cytosolic contamination (Fig. S6a). Additionally,
368 trypan blue staining of the infiltrated leaves revealed the absence of any cell damage and
369 potential cytosolic leakage (Fig.S7). Using size exclusion chromatography (SEC), the isolated
370 AWF was fractionated into 23 fractions (Fig. S2). Of these, fractions 1-7 contained the void
371 volume, fractions 8-11 contained EVs, and fractions 12-23 contained larger protein complexes.
372 Fractions 8-11, corresponding to EVs, were pooled together and examined using Transmission
373 Electron Microscopy (TEM) which confirmed the presence of vesicle-like structures at 50nm,
374 200nm, and 500nm size corresponding to the size of exosomes and micro-vesicular bodies in
375 plants (Rutter et al., 2017) (Fig. 1a). The pooled EV fractions were also subjected to Dynamic
376 Light Scattering (DLS) for particle size measurement, which revealed their size ranging 50 -1000
377 nm (Fig. 1b). Three peaks corresponding to the size 15nm, 100nm, and 500nm were obtained.
378 The percentage distribution for the 500nm size EVs was maximum compared to 100nm size EVs.

379 To examine the presence of ASSVd RNA in the apoplast and EVs, total RNA was isolated from
380 both AWF and pooled EV fractions. Given that RNA can be present either inside EVs or bound
381 to their surface as protein-associated RNA complexes (Karimi et al., 2022), the EVs were further
382 split into two fractions to pinpoint the localization of ASSVd RNA within these vesicles (Fig. 1c).
383 First, the EV fraction was treated with trypsin to release the protein associated RNA and the
384 RNA was isolated from the outer surface of the EVs without breaking the vesicles which
385 represented the RNA associated with the EV surface or EV outside RNA (EV^{O}). The remaining
386 EV fraction was treated with trypsin to remove proteins, followed by RNase treatment to degrade
387 protein-bound RNA from the EV surface. The EVs were then ruptured by treatment with
388 detergent and the inside RNA was isolated which represented the RNA inside EVs (EV^{I}). The
389 RT-PCR results indicated that ASSVd RNA is present in the apoplast, adhered to the surface of
390 EVs (as EV surface RNA), and is also found inside the EVs (Fig. 1d and 1e). However, the
391 intensity of the ASSVd band was weaker in the inside EV fraction compared to AWF and
392 outside EV fractions as also seen in the dot blot of the same RNA samples (Fig. 1f), suggesting
393 that the mature form of ASSVd RNA is present at lower concentrations inside the vesicles. To
394 further validate these findings, a denaturing Northern blot analysis of total RNA from AWF and
395 inside and outside EV fractions was carried out. The analysis revealed the presence of different

396 forms of ASSVd RNA (including circular, linear, and small RNAs) in both the apoplast and EV
397 fractions. Ethidium bromide staining of the denaturing PAGE gel with total RNA from AWF,
398 EV^O, and EV^I fractions showed an enrichment of small RNAs inside EVs compared to the other
399 fractions, consistent with earlier findings in Arabidopsis (Fig.1g) (Karimi et al., 2022).
400 Furthermore, the Northern blot results confirmed the presence of both circular and linear forms
401 of ASSVd RNA in the apoplast and in both the outer and inner EV fractions, implicating that
402 ASSVd RNA is indeed associated with EVs in these plants (Fig.1h and Table 1). Small RNA
403 species corresponding to ASSVd were detected only within the EVs, suggesting that ASSVd-
404 derived small RNAs (sRNAs) are packaged into these vesicles. The lack of probe hybridization
405 with the RNA from the mock leaf confirmed that the bands observed in the Northern blot were
406 specific to ASSVd and not from any other plant-derived RNAs.

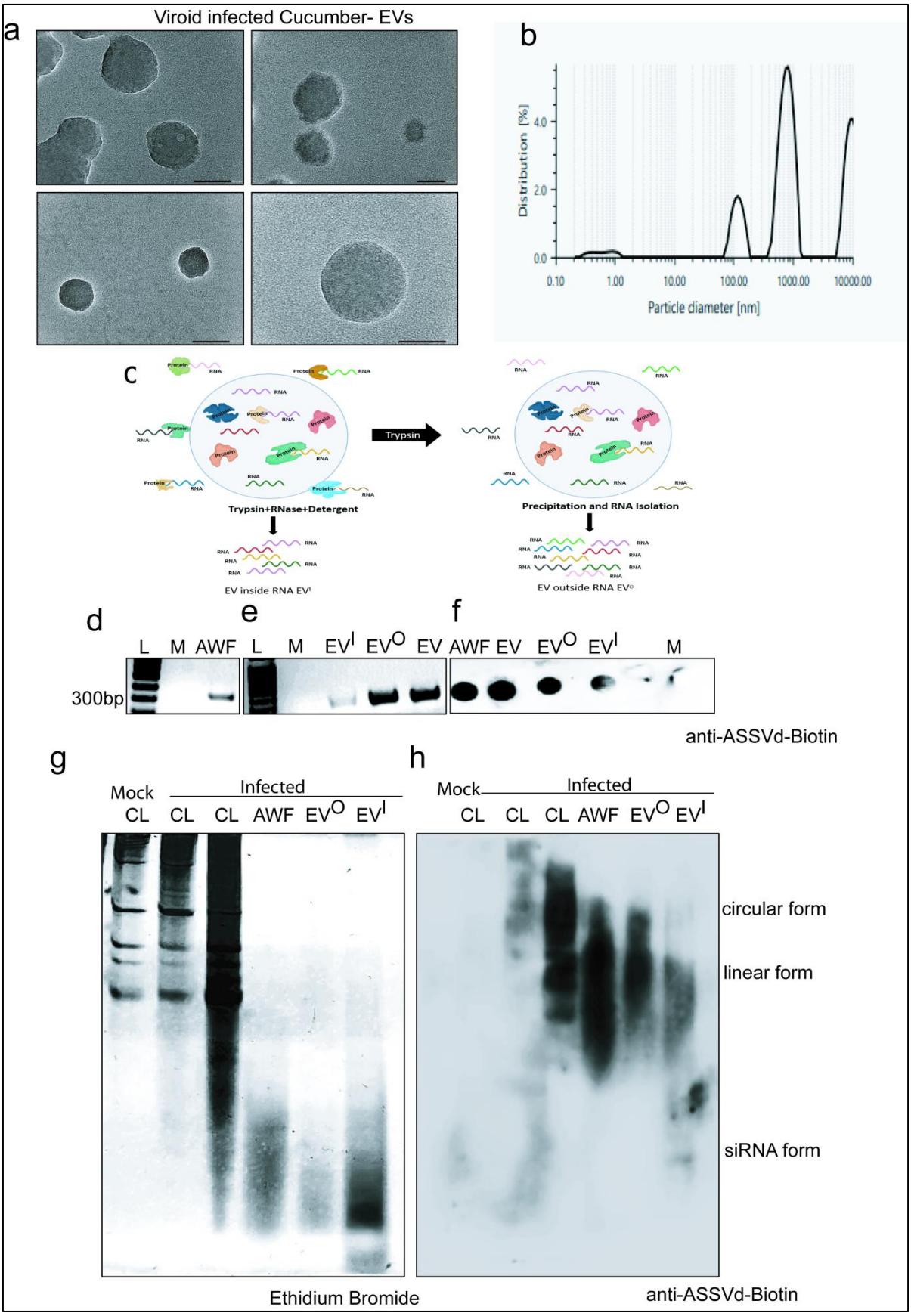
a
Viroid infected Cucumber- EVs
b
Distribution [%]
4.0
2.0
0.0
0.10
1.00
10.00
100.00
1000.00
10000.00
Particle diameter [nm]
c
Trypsin
Trypsin+RNase+Detergent
EV inside RNA EVI
Precipitation and RNA Isolation
EV outside RNA EVO
d
L M AWF
300bp
e
L M EVI EVO EV
f
AWF EV EVO EVI M
anti-ASSVd-Biotin
g
Mock
Infected
CL CL CL AWF EVO EVI
Ethidium Bromide
h
Mock
Infected
CL CL CL AWF EVO EVI
circular form
linear form
siRNA form
anti-ASSVd-Biotin

407

408 **Figure 1: Isolation and characterization of EVs from cucumber apoplast and detection of**
409 **ASSVd from apoplast and EVs**

410 (a) TEM images illustrating the morphology of EVs isolated from cucumber plants infected with
411 ASSVd using the SEC method. EVs are observed to range in size from 50 nm to 500 nm. (b) DLS
412 analysis of the isolated EVs showing particle sizes between 10 nm and 1000 nm, consistent with
413 the sizes observed in TEM. Each experiment was repeated thrice for validation. (c) Graphical
414 method illustrating the protocol followed for isolation of RNA from outside surface of EVs and
415 from EVs inside. (d, e and f) RT-PCR and dot blot detection of ASSVd in the AWF, total EV
416 fraction obtained via SEC (EV), EV^O fraction after trypsin treatment and RNA isolation without
417 EV disruption, and EV^I fraction after trypsin, RNase and detergent treatment followed by RNA
418 isolation from inside the EVs. (g and h) Northern blot analysis of the RNA samples described
419 above: left panel – EtBr-stained gel showing RNA from infected leaves and their corresponding
420 AWF and EV fractions, with mock leaf RNA as a control; right panel – Northern blot of the same
421 gel using a 3'-labeled biotin-negative sense ASSVd probe, revealing both circular and linear forms
422 of ASSVd in infected leaves, AWF, and inside and outside EVs. Small RNAs of ASSVd are
423 distinctly visible within the EV fraction. (Each experiment was repeated at-least three times for
424 validation)

Detection Technique	Detection by RT-PCR	Detection by Northern Blot		
Location/Form	Circular/Oligomeric form	Circular form	Linear form	SiRNA form
Apoplast	+	+	+	-
Outside EV surface	+	+	+	-
Inside EV	+	mild	Not detectable	+

425

426 **Table 1:** Representation of northern blot of denaturing PAGE of RNA hybridized with antisense
427 ASSVd probe 3' labeled with biotin which shows from mock cell lysate, viroid infected cell
428 lysate, viroid infected AWF, outside EVs (EV^O) and inside EVs (EV^I)

429

ASSVd RNA exhibits characteristics of EV loading including m6A modification and EXOmotifs

An immunoprecipitation (IP) experiment using antibodies specific to m6A with equal RNA from viroid-infected AWF and EVs (Fig. 2a) revealed distinct patterns of m6A modification. When the m6A enriched extracts were probed with biotin labeled negative sense ASSVd probe, it was observed that almost 50 percent RNA in the EVs is modified with m6A modification whereas in the apoplast almost 25 percent ASSVd RNA is in the m6A modified state. The remaining percent is either unmodified or modified with some other kind of modification. Thus, overall through these results, we infer that m6A modification of ASSVd could be one of the factors contributing to ASSVd RNA loading inside the EVs or export into the apoplast. Apart from m6A modification the presence of exosome sorting motifs (EXOmotifs) are also known to transport RNA into the vesicles. For this, we carried out a sequence-specific screening of ASSVd which revealed an enrichment of five EXOmotifs in the ASSVd genome viz. UCCC, CUCC, CCCU, UGUG, and GGUG (Fig. 2b). The UCCC and UGUG motifs lie in the terminal left domain, CUCC and CCCU lie in the central conserved region whereas GGUG lies in the pathogenicity domain of ASSVd (Fig. 2c).

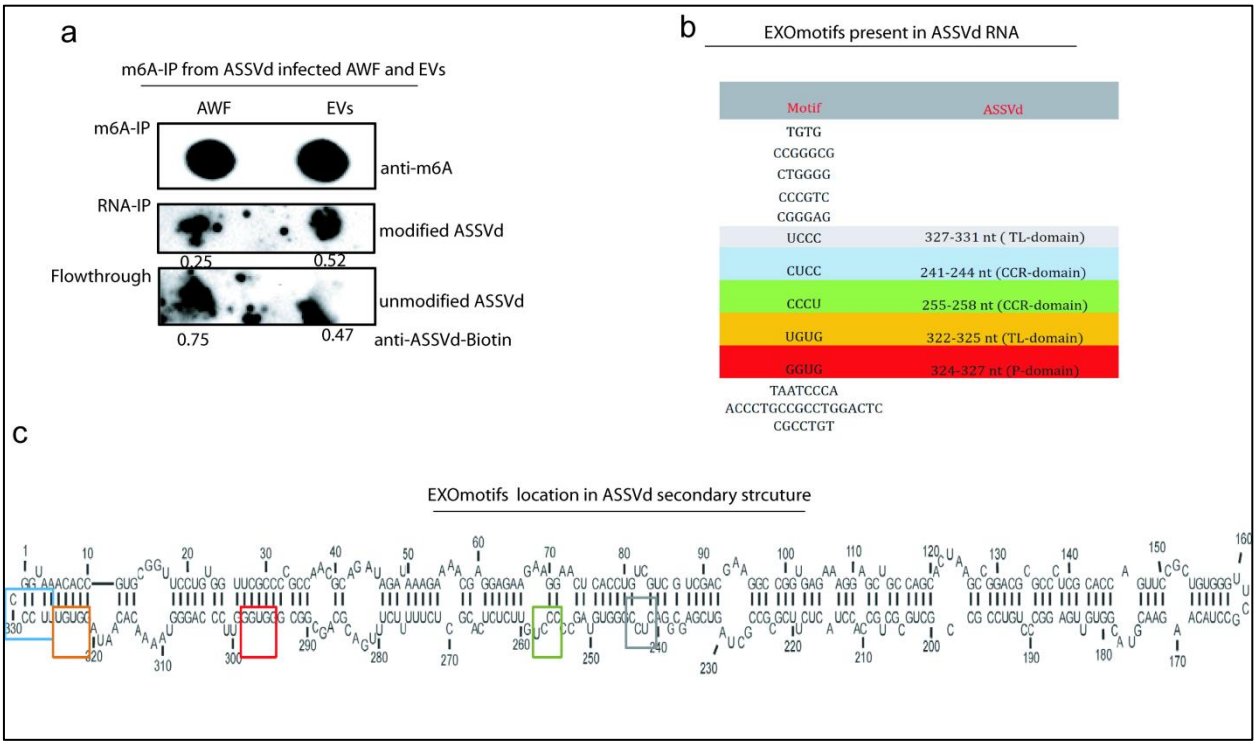

447 **Figure 2: Enrichment of m6A modification and EXOmotifs in the ASSVd genome.**

448 (a) Immunoprecipitation of m6A-enriched RNAs from the ASSVd-infected AWF and EVs
449 fractions using an m6A antibody (upper panel), followed by detection of ASSVd in the
450 immunoprecipitated samples using a 3'-labeled biotin-negative sense ASSVd probe (middle
451 panel). The middle panel shows that ASSVd RNA in EVs is modified with m6A, while the lower
452 panel demonstrates that unmodified ASSVd RNA, which did not bind to the m6A antibody,
453 remains in the flow-through fraction. (The assay was repeated twice to confirm the results) (b)
454 Overview of various EXOmotifs identified in animal studies from extracellular RNA and the
455 motifs found within the ASSVd genome. (c) The location of the identified EXOmotifs in the
456 secondary structure of ASSVd is highlighted by colored boxes.

457 **Investigating protein level changes in the cucumber EVs infected with viroid**

458 For the identification of protein changes in EVs upon viroid stress, EVs from AWF were isolated
459 from ASSVd-infected cucumber plants and mock plants three weeks post viroid infection (Fig.
460 S6b). The morphology of the isolated EVs was analyzed using TEM and DLS which revealed
461 EVs of size varying from 50nm to 1000nm (Fig. S8 and S9). Protein identification of the infected
462 and healthy EVs revealed proteins specific to exosomes such as tetraspanins (Tet16/PLAT/LH2
463 domain-containing lipoxygenase family protein) in healthy EVs, and lipoxygenase 3 (orthologue
464 of TET8 in cucumber) in infected EVs (Table 2). Additionally, markers for microvesicles,
465 including syntaxins (SYP21/71/31, SNARE-like superfamily protein) and target SNARE coiled-
466 coil domain protein in healthy EVs, and SYP124/21/42/71 and SNARE-like super-family
467 proteins were also found in infected EVs. Proteins associated with EXPO vesicles, such as
468 exocyst complex components (SEC84B, SEC15B, SEC5, EXO70 family protein in healthy EVs,
469 and SEC10, SEC15B in infected EVs) were also identified. These findings align with the TEM
470 data, which confirmed that EVs isolated through SEC had a size of 50-500nm consistent with the
471 size of exosomes, micro-vesicles, and EXPO vesicles in plants. Notably, enrichment of RNA-
472 binding proteins including Argonaute family proteins (AGO2, AGO3, and AGO7), DEAD-box
473 RNA helicases, sorting nexins, and glycine-rich RNA-binding proteins was also observed in both
474 healthy and infected plant EVs. Apart from these RNA-binding proteins, chaperonins such as
475 heat shock proteins (HSP60/70/81/89.1/70, DnaJ) were also identified in the EVs (Table 2).
476 Interestingly, a phloem protein -PP2 was also identified in the cucumber EVs which is known to

477 be involved in viroid transmission to whiteflies (Walia et al., 2015) and contains a dsRNA
478 binding motif. The absence of markers for the trans-Golgi network (syntaxin 61, SYP61), late
479 endosomes (Ara6), Golgi bodies (GmMan149), and plasma membrane (LTI6) confirmed the
480 integrity of the EVs and EV-specificity of the identified proteins (Table 2, File: S1 and S2). Gene
481 ontology (GO) enrichment analysis based on cellular components revealed that the proteins of
482 both healthy and infected EVs were associated with the endomembrane system, cell-cell
483 junctions, the apoplast, the plasma membrane, and extracellular space, among others (Fig.S10)
484 further confirming the purity of the isolated EVs. In the biological process category, the enriched
485 proteins in healthy EVs were primarily linked to the regulation of Ras protein signal transduction
486 and GTPase-mediated signal transduction, while infected EVs proteins were mainly involved in
487 cytoskeleton-dependent intracellular transport and microtubule-based movement (Fig. S11). A
488 deeper analysis of biological processes uncovered a particularly interesting finding: infected EVs
489 were notably enriched in proteins related to non-coding RNA processing/modification and RNA
490 processing/metabolic processes, a category not observed in healthy EVs.

	Healthy		Infected
Accession No.	**Protein name**	**Accession No**	**Protein name**
	Syntaxins related		
AT5G16830	Syntaxin of plants 21 (PEP12 VACULAOR TRANSPORT)	AT1G61290	Syntaxin of plants 124
AT3G09740	Syntaxin of plants 71	AT5G16830	Syntaxin of plants 21
AT5G05760	Syntaxin of plants 31	AT4G02195	Syntaxin of plants 42
AT5G02280	SNARE-like superfamily protein	AT5G02280	SNARE-like superfamily protein
AT1G15370	SNARE-like superfamily protein	AT2G35190	novel plant snare 11
AT1G16230	Target SNARE coiled-coil domain	AT1G16230	Target SNARE coiled-coil domain protein
		AT3G09740	syntaxin of plants 71
	Tetraspanin related		
AT3G22400	Lox5/PLAT/LH2 domain	AT1G17420	Lipoxygenase 3 (PLAT/LH2 domain)
AT1G18510	Tetraspanin 16 (TET8 RELATED)	AT4G02380	Senescence-associated gene 21
AT4G02380	Senescence-associated gene 21	AT2G29350	Senescence-associated gene 13
AT2G29350	Senescence-associated gene 13		
	EXPO Related		
AT5G49830	Exocyst complex component 84B	AT5G12370	Exocyst complex component sec10
AT4G02350	Exocyst complex component sec15B	AT2G32750	Exostosin family protein
AT2G28110	Exostosin family protein	AT4G02350	Exocyst complex component sec15B
AT1G21170	Exocyst complex component SEC5		
AT5G58430	Exocyst subunit exo70 family protein B1		
	RNA binding proteins		
AT1G69440	Argonaute family protein	AT1G31280	Argonaute family protein
AT1G31290	ARGONAUTE 3	AT1G31290	ARGONAUTE 3
		AT1G69440	Argonaute family protein
AT3G01540	DEAD box RNA helicase 1	AT5G26742	DEAD box RNA helicase (RH3)
AT5G07120	Sorting nexin 2B	AT5G07120	Sorting nexin 2B
AT1G15240	Sorting nexin, C-terminal	AT5G58440	Sorting nexin 2A
AT3G23830	Glycine-rich RNA-binding protein 4	AT3G23830	Glycine-rich RNA-binding protein 4
	Heat Shock proteins		
AT3G07770	HEAT SHOCK PROTEIN 89.1	AT3G13860	Heat shock protein 60-3A
AT1G11660	Heat shock protein 70 (Hsp 70)	AT1G11660	Heat shock protein 70 (Hsp 70)
AT4G02100	Heat shock protein DnaJ	AT3G07770	HEAT SHOCK PROTEIN 89.1
AT3G13860	Heat shock protein 60-3A	AT4G24280	Chloroplast heat shock protein 70-1
AT3G12580	Heat shock protein 70	AT3G23990	Heat shock protein 60
AT5G56030	Heat shock protein 81-2	AT3G08970	DNAJ heat shock N-terminal

	Proteasome components		
AT3G61140	Rpn7	AT1G04810	Rpn2/Psmd1 subunit
AT1G77440	20S Proteasome beta subunit C2	AT5G42790	Proteasome alpha subunit F1
AT1G13060	20S Proteasome beta subunit E1		
AT3G13330	Proteasome activating protein 200		
	Phloem Proteins		
		AT1G10155	Phloem protein 2-A10
		AT1G65390	Phloem protein 2 A5

Table 2: Displays the list of proteins identified in mass spectrometry data from both viroid-infected and healthy EVs. It includes plant EV-related proteins such as Syntaxins, Tetraspanins, and Expo proteins. Additionally, RNA-binding proteins and Heat shock proteins, previously reported to be associated with plant EVs, are also included. The table further highlights PP2 proteins identified specifically in the EVs from viroid-infected plants.

CsTET8 is a conserved EV marker protein in cucumber while CsPP2 is a newly identified RNA-binding protein localized within EVs

Mass-spectrometry results showed the presence of tetraspanins in cucumber EVs. We further confirmed the presence of TET8 (CsTET8) in cucumber EVs using immunoblotting. To determine whether Arabidopsis TET8 (AtTET8) antibodies cross-react with CsTET8, we conducted sequence analysis and found that the AtTet8 (AT2G23810) ortholog in cucumber, Tet8/Lipoxygenase domain 3 (Csa1g287020), shares 65.67% homology with AtTET8 (Fig. S12). Additionally, the 18 amino acids used to generate peptide-specific antibodies from the EC2 domain (Phytoab, USA) exhibited ~90% identity between Arabidopsis and cucumber Tet8, suggesting AtTET8 antibodies would likely recognize CsTET8 (Fig. S13).

To validate this, we transiently expressed CsTET8 (pSITE2CA-TET8 and HApBA-TET8) in *N. benthamiana* and performed immunoblotting with AtTET8 antibodies, confirming that AtTET8 effectively detects CsTET8 in cucumber plants (Figs. S14 and S15). Further western blot analysis using AtTET8 antibodies on cucumber samples detected a ~30 kDa band in cucumber

511 leaves and AWF, consistent with the expected size of AtTET8 in Arabidopsis (Figs. 3a and 3b).
512 These findings confirm that AtTET8 antibodies can effectively detect CsTET8 in cucumber.

513 To investigate the association of CsTET8 with cucumber EVs, various size-exclusion
514 chromatography (SEC) fractions were analyzed by western blotting. These fractions underwent a
515 protease protection assay: initially treated with trypsin to digest proteins exposed on the surface
516 of EVs, followed by detergent treatment to disrupt the vesicle membrane and release
517 intravesicular proteins. To further confirm the internal localization of specific proteins, EVs were
518 first lysed with detergent and then treated with trypsin, ensuring that only proteins within the
519 vesicles would be degraded.

520 CsTET8 was detected in EV-containing fractions F9 and F11, with the highest abundance in F11
521 (Fig. 3c, upper blot, first panel), indicating its presence within EVs. Trypsin treatment alone did
522 not significantly reduce the CsTET8 signal, particularly in F11, suggesting the protein is
523 protected from enzymatic digestion and therefore not exposed on the EV surface (Figs. 3c).
524 However, following vesicle disruption with detergent and subsequent trypsin treatment, CsTET8
525 bands were degraded, confirming its intravesicular localization (Fig. 3c, upper blot, second
526 panel).

527 Further validation came from the western blot analysis of pooled EV fractions (F9+F11), which
528 showed a strong CsTET8 signal on SDS-PAGE. This signal was significantly reduced after
529 detergent and trypsin treatment (Figs. 3d), and reflected in the corresponding intensities,
530 reinforcing that CsTET8 is sequestered within the EVs. These findings support that CsTET8 is
531 an integral, protected component of cucumber EVs, consistent with a conserved role across plant
532 species.

533 Another protein of interest was Phloem Protein 2 (CsPP2) which we proceeded further to explore
534 its association with the EVs. CsPP2 is a phloem lectin previously shown to interact with ASSVd
535 and assist in its cross-kingdom trafficking (Walia et al., 2015). Western blotting of cucumber cell
536 lysate and AWF confirmed the presence of CsPP2 in both intracellular and apoplastic
537 compartments (Fig. 3b). Analysis of SEC fractions revealed that CsPP2 co-eluted with CsTET8
538 in fractions F9 and F11 (Fig. 3c, lower panel). The protease protection assay demonstrated that

CsPP2 also resides within EVs: the intact band persisted after trypsin treatment but was degraded when EVs were pre-lysed with detergent before enzyme exposure (Figs. 3c and 3d). Furthermore, we transiently expressed CsPP2 fused with GFP in *Nicotiana benthamiana* and isolated EVs from the apoplast at 48 hpi. Fluorescence microscopy of the isolated EVs showed a distinct presence of GFP-CsPP2 in the EV fraction, in contrast to mock-treated plants (Fig. 3e and S16). Characteristic small, cup-shaped EV structures expressing GFP-CsPP2 were clearly observed. These findings collectively suggest that CsPP2 localizes both to the apoplast and within cucumber EVs, and when expressed in *N. benthamiana*, it retains the ability to associate with EVs.

Western blot analysis using plant Actin as a control confirmed the absence of Actin protein in both apoplastic and EV samples, verifying the purity of the EV preparations.

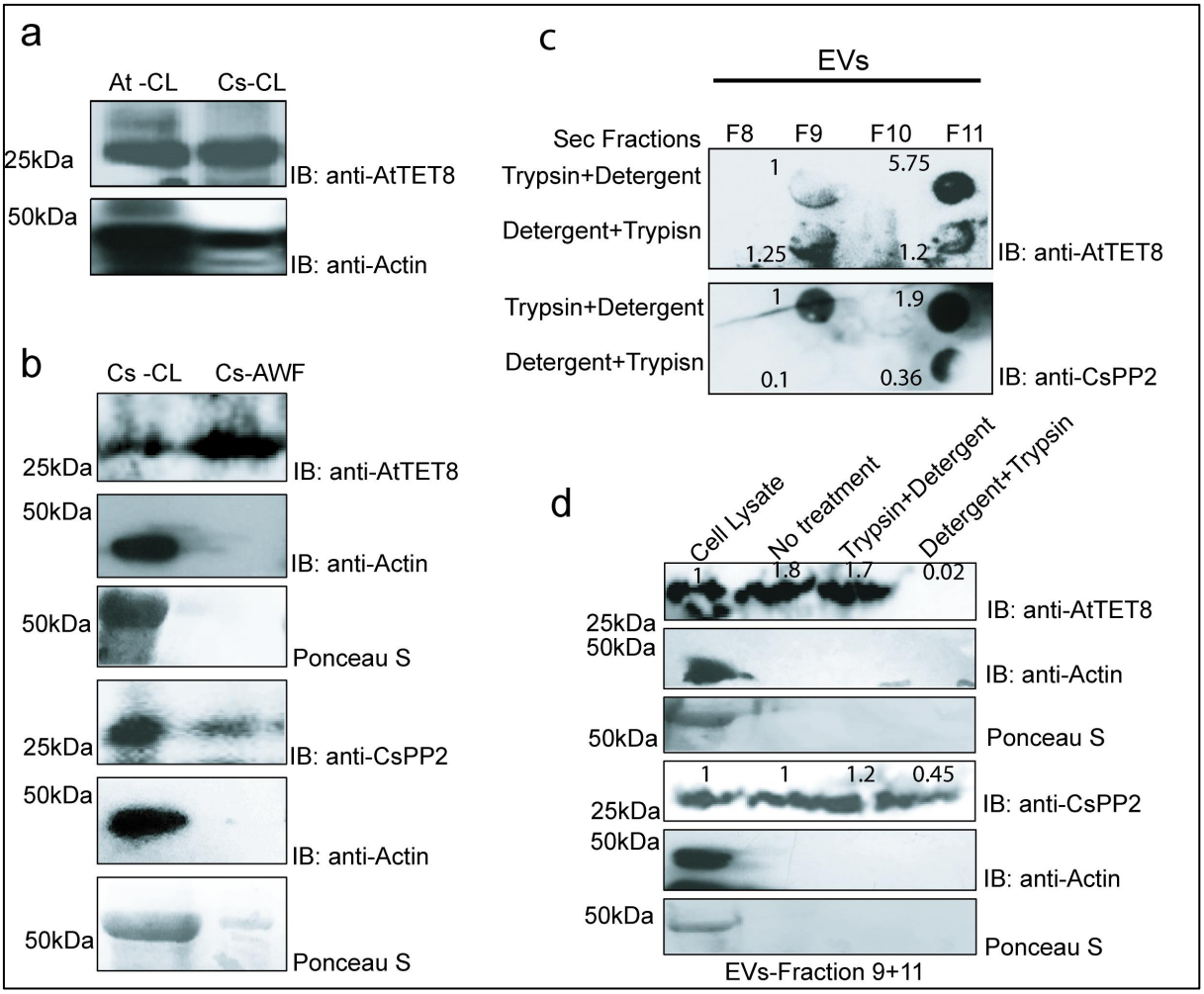

551

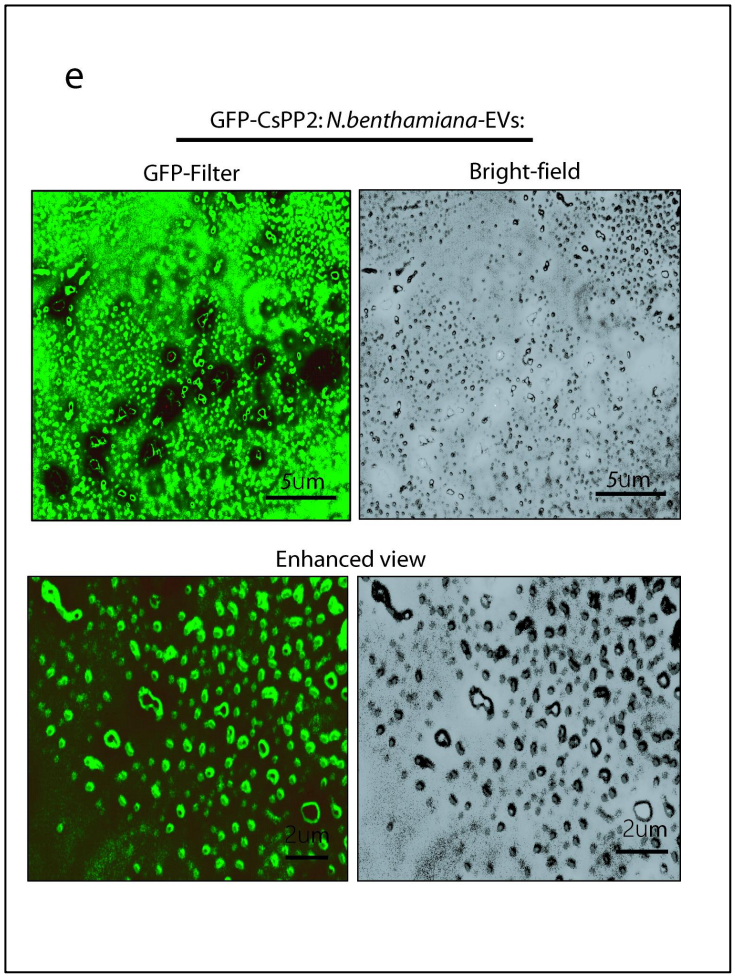

552

553 **Figure 3: Characterization of CsTET8 and CsPP2 from EVs infected with ASSVd.**

554 (a) Western blot detection of TET8 in arabidopsis cell lysate (At-CL) cucumber cell lysates (Cs-
555 CL) using Arabidopsis anti-AtTET8 antibody, revealing a band around 30 kDa, which
556 corresponds to the size of TET8 in both Arabidopsis and cucumber CL (lower panel) western
557 blot of the same extracts with anti-Actin antibody. (b) Western blot of cucumber CL and AWF
558 with anti-AtTET8 and anti-CsPP2 antibody. Western blot of the same extract with anti-actin
559 antibody are used as loading controls. (c)Western blot analysis of EV fractions (8-11) isolated by
560 SEC, using AtTET8 antibodies to detect CsTET8 and CsPP2 in fractions 9 and 11 (upper lane in
561 upper and lower blot). The fractions were treated with trypsin to degrade the surface proteins of
562 the EVs, followed by detergent-induced rupture before loading onto the membrane. The lower
563 lane shows the degradation of CsTET8 and CsPP2 from inside the EVs when ruptured with

564 detergent before trypsin digestion, suggesting both proteins are localized inside the EVs. (d)
565 Western blot analysis using anti-AtTET8 and anti-CsPP2 antibodies of pooled EV fractions (9
566 and 11) with different treatments—no treatment, trypsin followed by detergent, and detergent
567 followed by trypsin—indicating that CsTET8 and CsPP2 are localized both inside and outside
568 the EVs. Western blot of the same extract with anti-actin antibody are used as loading controls.
569 (Each experiment was repeated three to four times for validation) (e) Fluorescence microscopy
570 of EVs isolated from GFP-CsPP2 expressing *N.benthamiana* plants under GFP Filter and Bright
571 field (Scale bar 5ɥm and 2ɥm).

572 **CsPP2 may aid in the sorting of viroid and other plant RNAs into CsTET8-specific**
573 **exosomes**

574 The co-localization of CsTET8 and CsPP2 in the same EV fractions indicates a potential
575 interaction between these two. To validate this, we carried out immunoprecipitation of CsPP2
576 using CsPP2 antibody (Walia et al., 2015) from the total cell lysate and AWF (treated with
577 detergent to release the EV proteins) of viroid-infected plants and detected the presence of
578 CsTET8 in the pull-down sample. Our immunoblot analysis revealed the presence of CsTET8
579 protein in the CsPP2 immunoprecipitated from the cell lysate as well as extracellular fluid (Figs.
580 4a and 4b). To further validate the interaction, we performed a co-immunoprecipitation assay by
581 transiently co-expressing CsTET8 fused to GFP and CsPP2 fused to an HA tag using the binary
582 vectors pSITE2CA and HApBA, respectively. Immunoprecipitation of GFP-CsTET8 with anti-
583 GFP-conjugated beads resulted in a clear co-enrichment of HA-CsPP2, as detected by
584 immunoblotting with an anti-HA antibody, thereby confirming the interaction between the two
585 proteins (Fig. 4c-upper panel). The GFP pull-down alone did not immunoprecipitate the HA-PP2
586 (Fig. 4c-lower panel). Additionally, Bimolecular Fluorescence Complementation (BiFC) assays
587 revealed that the interaction occurs both in the cytoplasm and at the plasma membrane (Fig. 4d).
588 Interestingly we observed a punctate-like appearance near the plasma membrane indicating the
589 interactions between the two at plasma membrane (Fig. 4d). These punctate like appearance
590 were also observed when GFP-TET8 and GFP-PP2 were individually transiently expressed in *N.*
591 *benthamiana* plants (Fig. S17). In addition, the AlphaFold3 tool predicted a pTM score of 0.47
592 (close to a good structure score of 0.5) for the CsP2-CsTET8 interaction (Fig. 4e). The CsTET8
593 ortholog in Arabidopsis, TET8_ARATH, contains an extracellular domain (EC2) spanning

594 amino acids 97-235 and the CsPP2 likely interact with CsTET8 at its EC2 domain (Fig. 4e).
595 Overall, together these results validate the interaction between CsTET8 and CsPP2 in the
596 cucumber cell and apoplastic space.

597 Considering that CsPP2 is an RNA-binding protein, the interaction between CsTET8 and CsPP2
598 suggests that CsPP2 may play a role in sorting RNAs into CsTET8 exosomes. To explore this
599 interaction, total RNA was isolated from CsPP2-immunoprecipitated samples and the presence
600 of ASSVd RNA was detected by RT-PCR. The results confirmed the co-immunoprecipitation of
601 ASSVd RNA along with CsPP2 from the total cell lysate and apoplast (Fig. 4a and Fig. 4b).
602 Hence, these results suggested that CsPP2, ASSVd, and CsTET8 might exist as a trimeric
603 complex in cucumber plants. To get a deeper insight into this interaction we specifically carried
604 out immuno-enrichment of CsTET8 labeled exosomes from the total EV pool as reported in the
605 arabidopsis (He et al., 2021). Following enrichment, the exosomes were disrupted using
606 detergent and subjected to immunoblotting and RNA extraction. Immunoblot analysis of the
607 enriched CsTET8 exosomes revealed the co-presence of CsPP2, while RT-PCR of the same
608 extracts confirmed the presence of ASSVd within the CsTET8-specific exosomes (Fig. 4f).
609 Interestingly, when the enriched CsTET8 exosomes were analyzed without detergent-mediated
610 disruption, immunoblotting still detected CsPP2, but RT-PCR failed to detect ASSVd. This
611 suggests that ASSVd resides within the exosomes and that there is no direct interaction between
612 CsTET8 and ASSVd (Data not shown). We further validated this model through interactions
613 using Alphafold3, which revealed the tripartite interaction, in which CsPP2 interacts with the
614 viroid RNA on one side and CsTET8 on the other (Fig. 4g). However, CsTET8 did not show any
615 direct interaction with the viroid RNA. The model predicted the central conserved region (CCR)
616 of the viroid RNA, spanning nucleotides 81-96, was in closest proximity to CsPP2 at amino
617 acids 1-8, 41-47, and 91-101, with CsPP2 motifs spanning amino acids 41-47 and 91-101
618 containing known double-stranded RNA-binding motifs (dsRBM). Additionally, CsTET8 protein
619 motifs 186-193 and 208-211 were in close proximity to CsPP2 regions 78-86, 107-111, and 202-
620 206, which lie within the EC2 of CsTET8 (Fig. 4g). Thus, using a combination of biochemical
621 and bioinformatic tools, we demonstrate that CsTET8 specific exosomes harbor ASSVd and
622 CsPP2 where CsPP2-CsTET8 directly interact with each other at EC2 domain of CsTET8 but
623 there is no direct interaction between ASSVd-CsTET8 further supporting the notion that CsPP2
624 might facilitate loading of RNAs in CsTET8 specific exosomes. To further demonstrate that

625 CsPP2 could be a potential protein facilitating the sorting of RNAs inside EVs the CsPP2-
626 immunoprecipitated RNAs were separated using denaturing PAGE and stained with Diamond
627 nucleic acid stain, a binding between CsPP2 and RNAs of various sizes was observed in both
628 whole cell lysate and the apoplast/EV fractions (Fig. 4h)) further strengthening the role of CsPP2
629 as a RNA sorting protein inside vesicles.

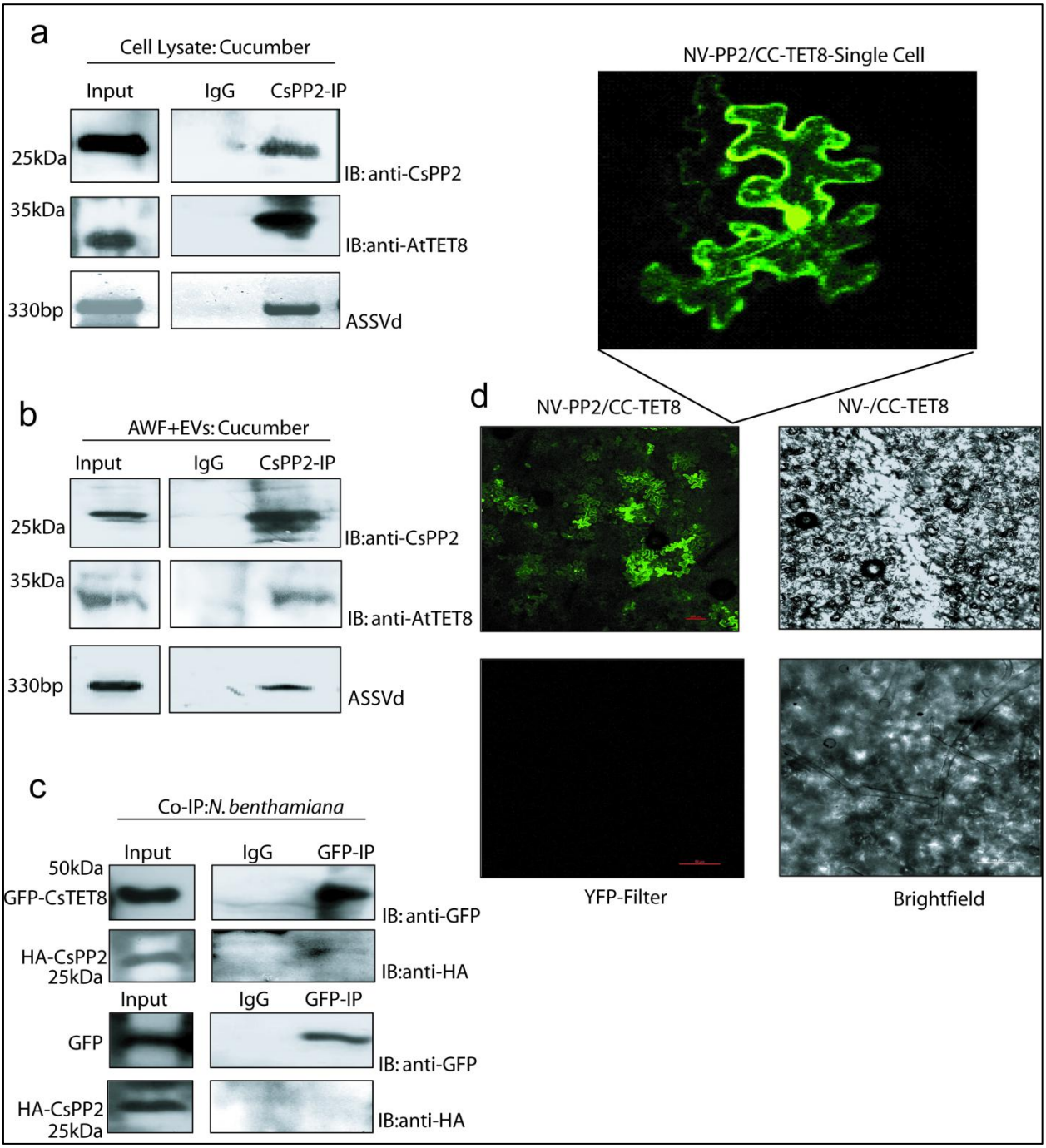

630

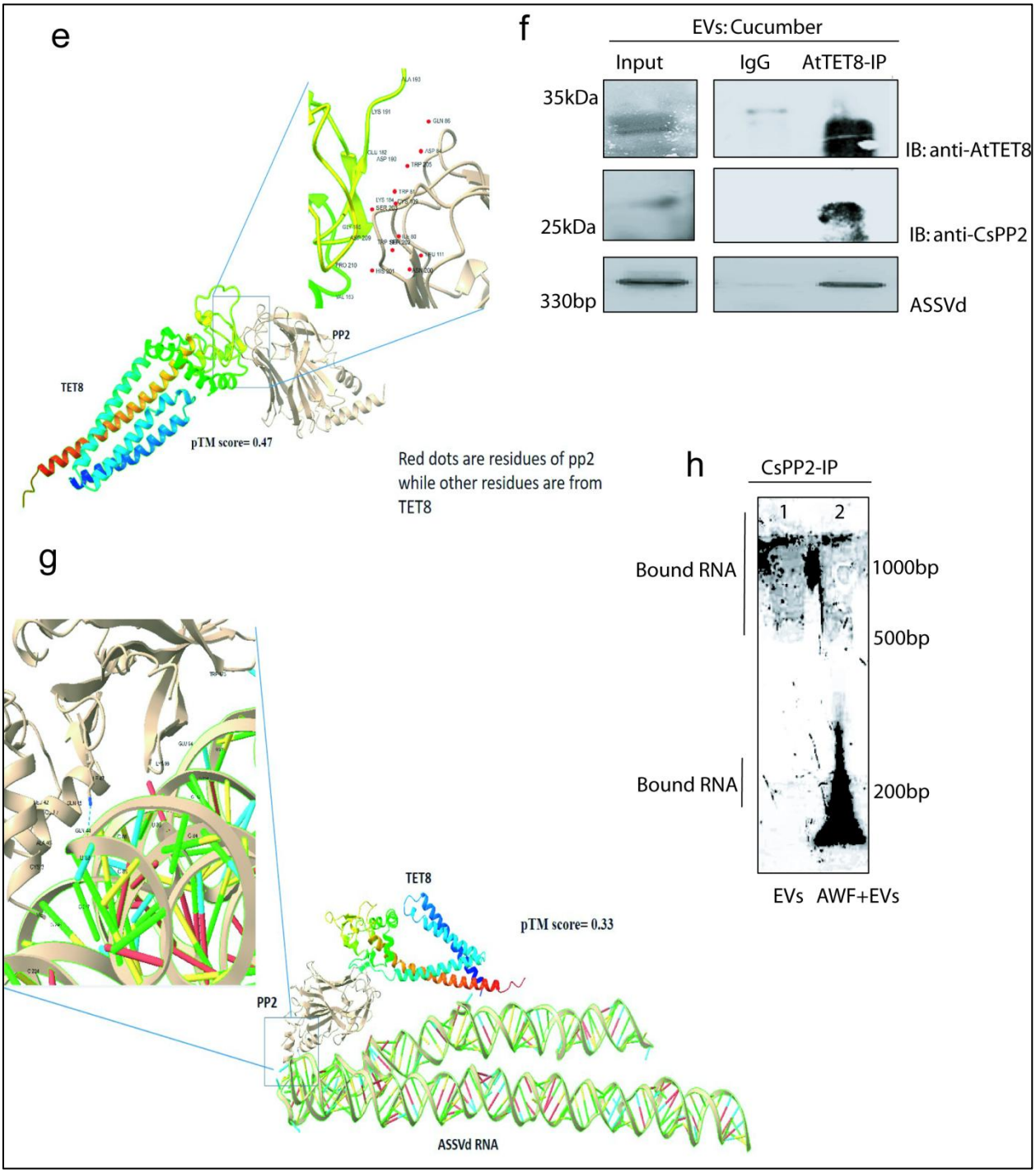

Figure 4: Interaction between CsPP2- CsTET8 and ASSVd

(a) Western blot analysis showing detection of CsPP2 in its immunoprecipitates from cell lysates (upper panel), along with co-detection of CsTET8 by western blot and ASSVd RNA by RT-PCR

636 from the same sample. **(b)** Western blot showing CsPP2 immunoprecipitated from the apoplast +
637 EVs fraction, with CsTET8 detected via western blot and ASSVd RNA via RT-PCR from the
638 same sample. **(c)** Western blot of a co-immunoprecipitation assay demonstrating the interaction
639 between GFP-TET8 and HA-PP2 when transiently expressed in *N. benthamiana*, using anti-GFP
640 and anti-HA antibodies. **(d)** BiFC images showing the interaction between CC-CsTET8 and NV-
641 CsPP2 observed under a YFP filter. Controls include CsTET8 and NV alone. Bright-field images
642 are shown alongside. A magnified image highlights punctate interaction near the plasma
643 membrane in a single cell. **(e)** Structural prediction of the CsTET8–CsPP2 interaction using
644 AlphaFold 3, with a pTM score of 0.47, suggesting a structure close to the true model. **(f)**
645 Western blot showing immuno-enrichment of CsTET8-containing exosomes from the total EV
646 pool, with co-detection of CsPP2 in the same sample. ASSVd RNA was also detected in the
647 immuno-enriched exosomes using RT-PCR. **(g)** The predicted interaction model of CsTET8,
648 CsPP2, and ASSVd using AlphaFold 3, with a pTM score of 0.33, indicating a model
649 approaching structural accuracy. RT-PCR confirmed the presence of ASSVd in infected samples.
650 **(h)** Total RNA extracted from CsPP2 immunoprecipitates was analyzed on a denaturing gel. The
651 right lane 1 represents RNA from leaf tissue and lane 2 from the apoplast + EVs fraction. Each
652 experiment was repeated at least three times to ensure reproducibility.

653 **Dynamics of CsPP2 and CsTET8 expression during viroid infection**

654 The expression of CsTET8 is known to be induced upon fungal infection in Arabidopsis (He et
655 al., 2021), while PP2 has been associated with plant defense (Zhang et al., 2011). To explore the
656 role of CsPP2 and CsTET8 upon viroid infection, we monitored the expression dynamics of
657 CsTET8 and CsPP2 proteins in plants infected with the ASSVd. Western blot analysis revealed a
658 gradual increase in CsTET8 expression from 7 to 28 dpi in ASSVd-infected plants, whereas
659 minimal expression was observed in mock-inoculated plants throughout the 21 days (Fig.6a and
660 6b). However, in viroid-infected plants, CsTET8 expression was elevated as early as 14 dpi,
661 indicating that ASSVd infection triggers the upregulation of CsTET8 at an earlier stage
662 compared to mock-infected plants. In parallel, immunoblot analysis of CsPP2 protein showed a
663 slight increase in expression following viroid infection, peaking at 7 dpi, before returning to
664 normal levels at 14 dpi and remaining constant throughout the infection period (Fig.5a). Hence,

665 both CsTET8 and CsPP2 respond to viroid infection but their expression dynamics differ from
666 each other.

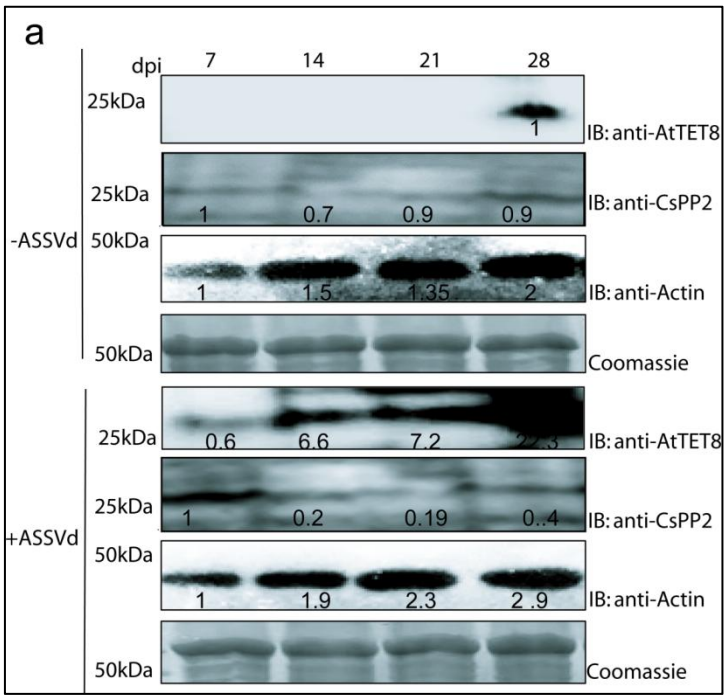

667

668 **Fig. 5: Dynamics of CsTET8 and CsPP2 upon viroid stress**

669 (a) Western blot analysis of mock-inoculated and viroid-infected cucumber plants at 7, 14, 21,
670 and 28 dpi, showing the expression levels of CsTET8, CsPP2, and Actin proteins. Blots were
671 probed with anti-CsPP2, anti-AtTET8, and anti-Actin antibodies. Coomassie staining of the same
672 extracts was performed to confirm equal protein loading across samples.

673 **EV-encapsulated ASSVd RNA is efficiently delivered via mechanical inoculation and is**
674 **readily acquired and transmitted by whiteflies**

675 To identify the role of EVs in viroid transmission, we conducted an experiment where a group of
676 ten whiteflies (*Trialeurodes vaporariorum*) were fed for 48 hours with three different treatments:
677 intact EVs, AWF (apoplast with EV fractions depleted), and water, in addition to an artificial diet
678 (Walia et al., 2015). After the feeding period, five whiteflies were analyzed for ASSVd presence
679 using RT-PCR, while the remaining five were allowed to feed on healthy cucumber plants. The
680 RT-PCR results revealed that whiteflies were able to acquire ASSVd from the intact EVs (Fig.

681 6a). Interestingly, a form of infectious ASSVd was also present in the apoplast that had been
682 depleted of EVs, and whiteflies were able to acquire it from there as well (Fig. 6a). However, the
683 PCR signal was significantly stronger for RNA acquired from intact EVs compared to that from
684 the apoplast, indicating that the viroid is more stable and protected from RNases when
685 encapsulated within EVs. This suggests that EVs might facilitate more efficient acquisition of the
686 viroid by whiteflies compared to naked RNA. No ASSVd was detected in whiteflies fed with
687 water.

688 Furthermore, plants that were fed with viroid-carrying whiteflies were tested for viroid
689 transmission at 14dpi using RT-PCR, which confirmed that the viroid could be actively acquired
690 and transmitted from EVs through the whiteflies (Fig. 6b). Additionally, we demonstrated that
691 mechanical inoculation of healthy cucumber plants with EVs could also deliver the viroid. For
692 this, we inoculated healthy cucumber plants with intact EVs, AWF, or water. At 14 dpi, RT-PCR
693 on the plants confirmed the presence of ASSVd infection, showing that both the apoplast and
694 EVs of infected plants contained infectious forms of the viroid (Fig. 6c). In contrast, plants
695 inoculated with water showed no viroid-specific amplification. Overall our results suggest that
696 EV-encapsulated viroid RNA can be readily acquired and transmitted by whiteflies to healthy
697 plants.

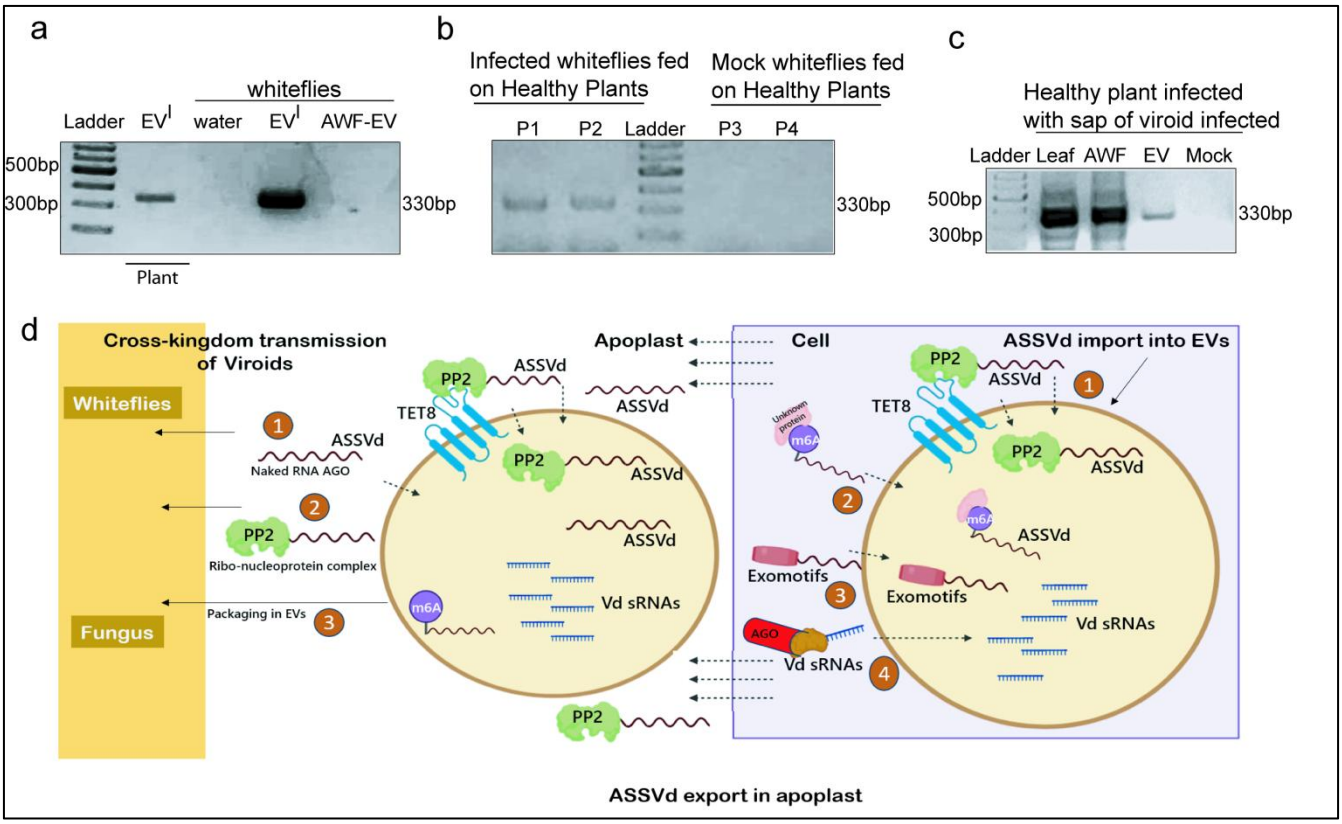

Figure 6: Active transmission of ASSVd to healthy plants and whiteflies via infected EVs.

(a) RT-PCR showing detection of the viroid within EVs, whiteflies fed with intact EVs, apoplast lacking EVs, and water as the mock control. (b) RT-PCR showing detection of ASSVd in plants fed with whiteflies that were pre-fed on viroid-infected EVs, with water serving as the control. (c) RT-PCR analysis of cucumber plant sap inoculated with leaf tissue, AWF, and EVs from viroid-infected plants, revealing a 330 bp amplification corresponding to the ASSVd genome using viroid-specific primers. Plants inoculated with water, used as a mock control, did not show the presence of the viroid, serving as a negative control in the assay. (d) A graphical summary of the key findings from the study. In brief, ASSVd RNA (both circular and linear forms) and VdsRNAs can be packaged into EVs. PP2 interacts with ASSVd RNA and the EC2 domain of TET8 within the cell, potentially facilitating the packaging of ASSVd RNAs into EVs. Additionally, ASSVd RNA is modified with m6A inside the cell and contains exomotifs that may aid in its loading into EVs. Once inside the EVs, the viroid RNA is transported to the extracellular space via these vesicles. Viroid RNAs also exist in the apoplast independently of EVs, either as naked RNA species or as RNP complexes. These viroid RNAs can be acquired by

714 whiteflies, and likely by fungi as well, in the form of EV-encapsulated RNA or naked RNAs as
715 RNP complexes, and then transmitted to healthy plants. (The experiment was repeated twice and
716 performed with a set of biological replicates).

717 **Discussion**

718 Viroids, unlike bacteria and fungi, are intracellular pathogens that replicate within the nucleus or
719 chloroplast of the cell. They traffic cell to cell through cytoplasmic connections, plasmodesmata,
720 and through phloem-mediated routes for their long-distance movement. Our previous studies
721 have highlighted the potential role of viroids in cross-kingdom trafficking, such as the
722 acquisition and transmission of ASSVd RNA by whiteflies to neighboring plants (Walia et al.,
723 2015). Later, this phenomenon was also reported in natural interactions between apple plants and
724 their fungal pathogens (Tian et al., 2022). These observations, combined with research on the
725 role of EVs in RNA trafficking during plant-fungal interactions (Cai et al., 2018; Wang et al.,
726 2024), raised important questions about whether the viroid RNAs, typically considered
727 intracellular pathogens, could also be transported in EVs. Our study aimed to investigate the
728 presence of ASSVd RNA in the extracellular space including EVs. Interestingly, our results
729 revealed that viroid RNA also exists in the apoplast, and different forms of ASSVd RNA—
730 circular, linear, and small RNAs—are packaged into the EVs of cucumber plants. This indicated
731 that viroids may employ EVs for *in planta* and cross-kingdom trafficking, as EVs could protect
732 the RNA from host RNases and help viroids cross biological barriers. In animals, certain factors
733 have been identified that assist in the selective loading of RNAs into EVs. For example, certain
734 sequences have been identified in animals that code for the loading of microRNAs into EVs
735 (Martin et al., 2022). These motifs are referred to as EXOmotifs. In search for the identification
736 of such factors that could preferentially facilitate the transport and packaging of viroid RNAs
737 inside EVs, we observed an enrichment of five EXOmotifs in the ASSVd genome. Interestingly,
738 sequence-specific screening of most of the viroids revealed a pattern of exomotif enrichment in
739 their genomes (Fig. S18). For example, the UGUG motif is present in 24 out of 30 viroids,
740 CGGGAG in 2 out of 30, CCGGGG in 16 out of 30, and CCGGUG in 20 out of 30. Notably, the
741 majority of viroids, on average, possess five enriched exomotifs in their genomes. Furthermore,
742 the 25-nt long ACCCUGCCGCCUGGACUCCGCCUGU motif is specifically present in TASVd,
743 which is known to be transmitted by bumblebees through encapsulation in potato leaf roll virus.

744 Apart from EXOmotifs in animals as well as in plants, the m6A modification of RNA has been
745 linked to the sorting of RNAs into EVs. For example, it has been reported that m6A modification
746 of miRNAs alters their binding affinity to AGO1 protein and increases their association with
747 RNA-binding proteins subsequently facilitating their extracellular export (Sabrina Garbo et al.,
748 2024). In plants, the apoplastic localized circular RNAs and long noncoding RNAs are enriched
749 in m6A which likely facilitates their export into EVs (Karimi et al., 2022). In this study, we
750 found that most EV-localized viroid RNA is modified with m6A however, which of the three
751 forms, whether circular, linear, or small RNA form is modified with m6A still needs to be
752 investigated. Although the biological relevance of this modification is unclear, it is possible that
753 it might have implications on viroid encapsulation within the EVs. Some viroid RNAs are known
754 to undergo reversible modifications, such as m6A methylation (Pavel Vopalensky et al., 2024),
755 thus it is plausible that ASSVd RNA is modified with m6A to enhance its export.

756 An intriguing finding of our study is the identification of CsPP2, a phloem-specific protein, in
757 the apoplast and EVs of cucumber. A recent study examining the enrichment of the 26S
758 proteasome from melon EVs reported the presence of PP2 in EVs from aphid-infested plants
759 (Sánchez López, 2024). This suggests that the localization of PP2 in the EVs of the
760 *Cucurbitaceae* species could represent a conserved phenomenon. CsPP2 is a phloem lectin with
761 dsRNA binding motifs, capable of increasing the size exclusion limit of plasmodesmata, and has
762 been implicated in the movement of various endogenous and pathogenic RNAs within the
763 phloem (Gomez and Pallas, 2004). In our previous work, we demonstrated that the viroid-PP2
764 complex is more efficiently acquired and transmitted by whiteflies compared to the naked viroid
765 RNAs (Walia et al., 2015). In the current study, through a feeding assay of EVs to whiteflies, we
766 observed that viroid RNA is acquired and transmitted more efficiently by the whiteflies when
767 packaged into EVs rather than naked RNA or as an RNP complex. This suggests that although
768 viroid RNA can be acquired by whiteflies in various forms—either as a free RNA molecule, an
769 RNP complex or encapsulated within EVs—the transmission through EVs provides a dual
770 advantage: protection from host RNases and a safer route into new host kingdoms. Interestingly,
771 it has been proposed that cross-kingdom trafficking of RNAs can occur via both EVs and RNP
772 complexes. One research group reported that RNA-binding proteins such as AGO1, RNA
773 helicases, and annexins can mediate RNA loading into vesicles and facilitate subsequent cross-
774 kingdom trafficking (He et al., 2021; Cai et al., 2019; Wang et al., 2024). Additionally, another

775 group demonstrated that apoplast-localized proteins like GRP7 and AGO2 can bind to the RNAs
776 in the apoplast, potentially aiding in the cross-kingdom movement of RNAs as RNP complexes
777 (Karimi et al., 2022). Combining these findings, we show using viroid RNA as a model, that
778 cross-kingdom trafficking of RNAs can occur both as RNP complexes and via EVs, although
779 potentially at different intensities. However, the relevance and function of viroid RNAs and
780 CsPP2 within EVs, as well as the potential for viroids to be transmitted through EV
781 encapsulation, require further investigation. The presence of the CsPP2-viroid complex in the
782 apoplast and its association with CsTET8 suggests that CsPP2 may be a novel protein that assists
783 in sorting RNA into EVs in *Cucurbitaceae* plants. Interestingly like TET8, CsPP2 also exhibits
784 the presence of a transmemberane domain in its structure which supports its presence in the
785 extracellular space and EVs (Fig. S19). It is quite possible that viroids can channelize the EV-
786 mediated route for their systemic movement inside plants, as hypothesized for the movement of
787 endogenous RNAs and viral RNAs in plants (Kehr et al., 2018).

788 The EV proteins from viroid-infected plants implicated changes in nuclear proteins specifically
789 related to non-coding RNA-related biological processes. Viroids are nuclear-replicating
790 pathogens and their effect on nuclear protein turnover and their subsequent export via autophagy
791 or extracellular vesicles warrant further investigation. These findings correlate with cancer
792 disease progression, where genomic DNA and nuclear components are exported by the formation
793 of amphisome-like structures and their fusion to vesicles (Akira et al., 2019). It is quite possible
794 that viroids may influence similar processes during infection, and hence, characterization of
795 DNA and RNA from EVs during viroid infection might shed light on these unexplored processes
796 related to viroid pathogenicity in plants. The induced expression of CsTET8 and CsPP2 proteins
797 suggests that it acts as a positive regulator of viroid stress and could be used as a marker protein
798 for viroid stress. Overall, through our study using ASSVd as the model RNA system, cucumber
799 as its host, and whitefly as its vector, we propose that viroid RNAs are exported into the plant
800 apoplast and packaged into EVs from where they can be acquired by the whiteflies (Fig. 6d).
801 They may use EVs as a means of cross-kingdom trafficking and their interactions with RNA-
802 binding proteins such as CsPP2 could assist their loading into exosomes which improve their
803 transmission efficiency. Moreover, the presence of factors like EXOmotifs or m6A modification
804 may assist viroid RNA in their packaging inside EVs. The precise functional roles of small
805 RNAs in EVs, particularly those derived from viroids and their characterization, remain unclear.

806 These small RNAs may influence the plant's immune response or aid in the viroid's transmission
807 to other organisms, such as insects or fungi. Understanding the mechanisms by which viroids and
808 other RNA molecules are sorted into vesicles and transferred across biological boundaries will
809 offer valuable insights into cross-kingdom RNA trafficking, with implications for viroid biology,
810 RNA-based inter-organism communication, and the ecological impact of RNA transfer.

811 **Author contributions**

812 **Neha Devi:** Formal analysis, methodology, and validation. **Vasudha Sharma**: Formal analysis
813 and methodology. **Nisha Devi:** Formal analysis and methodology. **Ravi Gupta:** writing-
814 reviewing, and editing (supporting). **Sunny Dhir:** conceptualization, data analysis, investigation,
815 methodology, supervision (equal), writing- review and editing. **Yashika Walia:**
816 conceptualization (lead), data curation and analysis (lead), investigation (lead), methodology,
817 supervision (equal), validation, writing- original draft, writing- review and editing, funding
818 acquisition.

819 **Acknowledgments**

820 We would like to thank the Management MMDU, for providing necessary research facilities. We
821 would like to acknowledge iSTEM facility at SAIF, IIT Bombay for mass-spectrometry analysis
822 and CIL facility at Panjab University Chandigarh for TEM imaging and Confocal analysis. We
823 would also like to thank I-STEM facility at Jamia Hamdard, New Delhi for confocal microscopy.
824 We acknowledge special thanks to Dr. Vipin Hallan, CSIR-IHBT Palampur for providing CsPP2
825 antibodies.

826

827 **Funding**

828 The work was supported by State University Research Excellence Award to Dr. Yashika Walia
829 and Dr. Sunny Dhir by Anusandhan National Research Foundation (ANRF), Government of
830 India through project number SUR/2022/001747. We also thanks to Department of
831 Biotechnology, and Government of India through EMR grant
832 BT/PR40936/AGIII/103/1255/2020 to Dr. Sunny Dhir and to Bayer for providing MEDHA
833 fellowship to Ms. Nisha Devi.

834 **Disclosure of Interest:** The authors report no conflict of interest

835 **Ethics Statement:** not applicable

836 **Data availability statement:** The data that support the findings of this study are available from
837 the corresponding author (YW) upon reasonable request.

838 **References**

839 1. Wang, S., et al., *Plant mRNAs move into a fungal pathogen via extracellular vesicles to*
840 *reduce infection.* Cell host & microbe, 2024. **32**(1): p. 93-105. e6.
841 2. Zhang, M., et al., *Plant derived edible nanoparticles as a new therapeutic approach*
842 *against diseases.* Tissue barriers, 2016. **4**(2): p. e1134415.
843 3. Zand Karimi, H., et al., *Arabidopsis apoplastic fluid contains sRNA-and circular RNA–*
844 *protein complexes that are located outside extracellular vesicles.* The Plant Cell, 2022.
845 **34**(5): p. 1863-1881.
846 4. He, B., et al., *RNA-binding proteins contribute to small RNA loading in plant*
847 *extracellular vesicles.* Nature plants, 2021. **7**(3): p. 342-352.
848 5. Ambrosone, A., et al., *Plant extracellular vesicles: Current landscape and future*
849 *directions.* Plants, 2023. **12**(24): p. 4141.
850 6. Chen, A., B. He, and H. Jin, *Isolation of extracellular vesicles from arabidopsis.* Current
851 protocols, 2022. **2**(1): p. e352.
852 7. Jankovičová, J., et al., *Tetraspanins, more than markers of extracellular vesicles in*
853 *reproduction.* International Journal of Molecular Sciences, 2020. **21**(20): p. 7568.
854 8. Rutter, B.D. and R.W. Innes, *Extracellular vesicles isolated from the leaf apoplast carry*
855 *stress-response proteins.* Plant physiology, 2017. **173**(1): p. 728-741.
856 9. Wang, J., et al., *EXPO, an exocyst-positive organelle distinct from multivesicular*
857 *endosomes and autophagosomes, mediates cytosol to cell wall exocytosis in Arabidopsis*
858 *and tobacco cells.* The Plant Cell, 2010. **22**(12): p. 4009-4030.
859 10. Ding, Y., et al., *Exo70E2 is essential for exocyst subunit recruitment and EXPO*
860 *formation in both plants and animals.* Molecular biology of the cell, 2014. **25**(3): p. 412-
861 426.
862 11. Weiberg, A., et al., *Fungal small RNAs suppress plant immunity by hijacking host RNA*
863 *interference pathways.* Science, 2013. **342**(6154): p. 118-123.

12. Cai, Q., et al., *Plants send small RNAs in extracellular vesicles to fungal pathogen to silence virulence genes.* Science, 2018. **360**(6393): p. 1126-1129.
13. Garbo, S., et al., *m6A modification inhibits miRNAs' intracellular function, favoring their extracellular export for intercellular communication.* Cell Reports, 2024. **43**(6).
14. O'Grady, T., et al., *Sorting and packaging of RNA into extracellular vesicles shape intracellular transcript levels.* BMC biology, 2022. **20**(1): p. 72.
15. Garcia-Martin, R., et al., *MicroRNA sequence codes for small extracellular vesicle release and cellular retention.* Nature, 2022. **601**(7893): p. 446-451.
16. Liu, Y.-f., et al., *CYP2A6 suppresses hepatocellular carcinoma via inhibiting SRC/Wnt/β-Catenin pathway.* Acta Pharmacologica Sinica, 2025: p. 1-12.
17. Flores, R., R.A. Owens, and J. Taylor, *Pathogenesis by subviral agents: viroids and hepatitis delta virus.* Current opinion in virology, 2016. **17**: p. 87-94.
18. Navarro, B., R. Flores, and F. Di Serio, *Advances in viroid-host interactions.* Annual Review of Virology, 2021. **8**(1): p. 305-325.
19. Hammond, R.W., *Economic significance of viroids in vegetable and field crops*, in *Viroids and satellites*. 2017, Elsevier. p. 5-13.
20. Branch, A.D. and H.D. Robertson, *A replication cycle for viroids and other small infectious RNA's.* Science, 1984. **223**(4635): p. 450-455.
21. Warrilow, D. and R. Symons, *Citrus exocortis viroid RNA is associated with the largest subunit of RNA polymerase II in tomato in vivo.* Archives of virology, 1999. **144**: p. 2367-2375.
22. Navarro, J.A. and R. Flores, *Characterization of the initiation sites of both polarity strands of a viroid RNA reveals a motif conserved in sequence and structure.* The EMBO Journal, 2000.
23. Rodio, M.-E., et al., *A viroid RNA with a specific structural motif inhibits chloroplast development.* The Plant Cell, 2007. **19**(11): p. 3610-3626.
24. Daròs, J.-A., et al., *Replication of avocado sunblotch viroid: evidence for a symmetric pathway with two rolling circles and hammerhead ribozyme processing.* Proceedings of the National Academy of Sciences, 1994. **91**(26): p. 12813-12817.

893 25. Sano, T., et al., *Identification of multiple structural domains regulating viroid*
894 *pathogenicity.* Proceedings of the National Academy of Sciences, 1992. **89**(21): p.
895 10104-10108.
896 26. Reanwarakorn, K. and J. Semancik, *Regulation of pathogenicity in hop stunt viroid-*
897 *related group II citrus viroids.* Journal of General Virology, 1998. **79**(12): p. 3163-3171.
898 27. SCHMITZ, A. and D. RIESNER, *Correlation between bending of the VM region and*
899 *pathogenicity of different potato spindle tuber viroid strains.* RNA, 1998. **4**(10): p. 1295-
900 1303.
901 28. Schnölzer, M., et al., *Correlation between structure and pathogenicity of potato spindle*
902 *tuber viroid (PSTV).* The EMBO Journal, 1985. **4**(9): p. 2181-2190.
903 29. Afanasenko, O., et al., *Transmission of potato spindle tuber viroid between Phytophthora*
904 *infestans and host plants.* Vavilov Journal of Genetics and Breeding, 2022. **26**(3): p. 272.
905 30. Leichtfried, T., et al., *Apple chlorotic fruit spot viroid: a putative new pathogenic viroid*
906 *on apple characterized by next-generation sequencing.* Archives of Virology, 2019. **164**:
907 p. 3137-3140.
908 31. Walia, Y., et al., *Apple scar skin viroid naked RNA is actively transmitted by the whitefly*
909 *Trialeurodes vaporariorum.* Rna Biology, 2015. **12**(10): p. 1131-1138.
910 32. Tian, M., et al., *Natural cross-kingdom spread of apple scar skin viroid from apple trees*
911 *to fungi.* Cells, 2022. **11**(22): p. 3686.
912 33. Walia, Y., et al., *Identification of the herbaceous host range of Apple scar skin viroid and*
913 *analysis of its progeny variants.* Plant pathology, 2014. **63**(3): p. 684-690.
914 34. O'Leary, B.M., et al., *The infiltration-centrifugation technique for extraction of*
915 *apoplastic fluid from plant leaves using Phaseolus vulgaris as an example.* Journal of
916 visualized experiments: JoVE, 2014(94): p. 52113.
917 35. Vopalensky, P., et al., *Exploring RNA modifications in infectious non-coding circular*
918 *RNAs.* RNA biology, 2025(just-accepted).
919 36. Sánchez-López, C.M., et al., *Phloem sap from melon plants contains extracellular*
920 *vesicles that carry active proteasomes which increase in response to aphid infestation.*
921 Journal of Extracellular Vesicles, 2024. **13**(10): p. e12517.

37. Gomez, G., H. Torres, and V. Pallas, *Identification of translocatable RNA-binding phloem proteins from melon, potential components of the long-distance RNA transport system.* The Plant Journal, 2005. **41**(1): p. 107-116.

38. Kehr, J. and F. Kragler, *Long distance RNA movement.* New Phytologist, 2018. **218**(1): p. 29-40.

39. Yokoi, A., et al., *Mechanisms of nuclear content loading to exosomes.* Science advances, 2019. **5**(11): p. eaax8849.

951 **Supporting data**

952

953 **Selective packaging of pathogenic non-coding RNAs into plant exosomes mediated through**
954 **Phloem Protein 2 and Tetraspanin 8 may represent a key mechanism for their cross-**
955 **kingdom transmission**

956 Neha Devi[1], Nisha Devi[1], Vasudha Sharma[1], Ravi Gupta[2], Sunny Dhir[1]*, Yashika Walia[1]*

957 [1]Molecular Plant Virology Group, R&D Lab, Department of Bio-Sciences & Technology,
958 Maharishi Markandeshwar (Deemed to be University), Mullana, Ambala-133207 HR India

959 [2]Plant Stress Physiology and Proteomics Laboratory, College of General Education, Kookmin
960 University, Seoul, South Korea

961 Neha Devi: nehadevi611999@gmail.com

962 Vasudha Sharma: vasu.3096sharma@gmail.com

963 Nisha Devi: nishapahal99@gmail.com

964 *Corresponding Authors

965 Dr. Yashika Walia; yashikawalia@gmail.com, yashika.dhir@mmumullana.org

966 ORCID ID: 0000-0002-0796-0050

967 Dr. Sunny Dhir; sunny72155@gmail.com, sunny.dhir@mmumullana.org

968 ORCID ID: 0000-0002-3790-8333

969

970

971

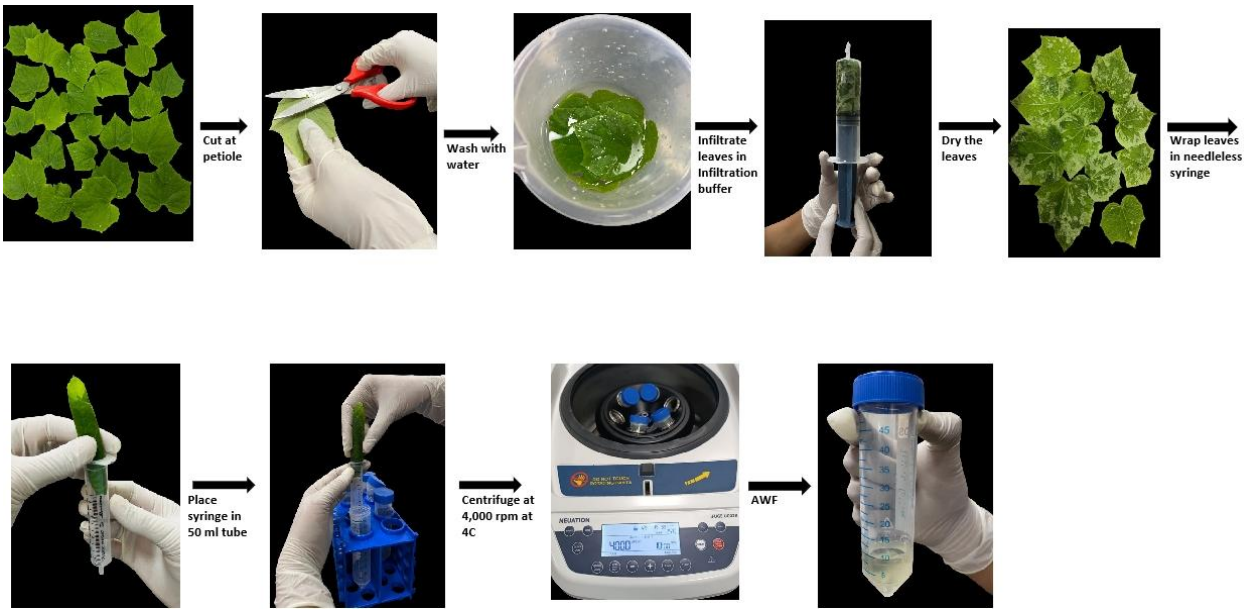

Fig. S1 showing the procedure followed for isolation of AWF from cucumber leaves

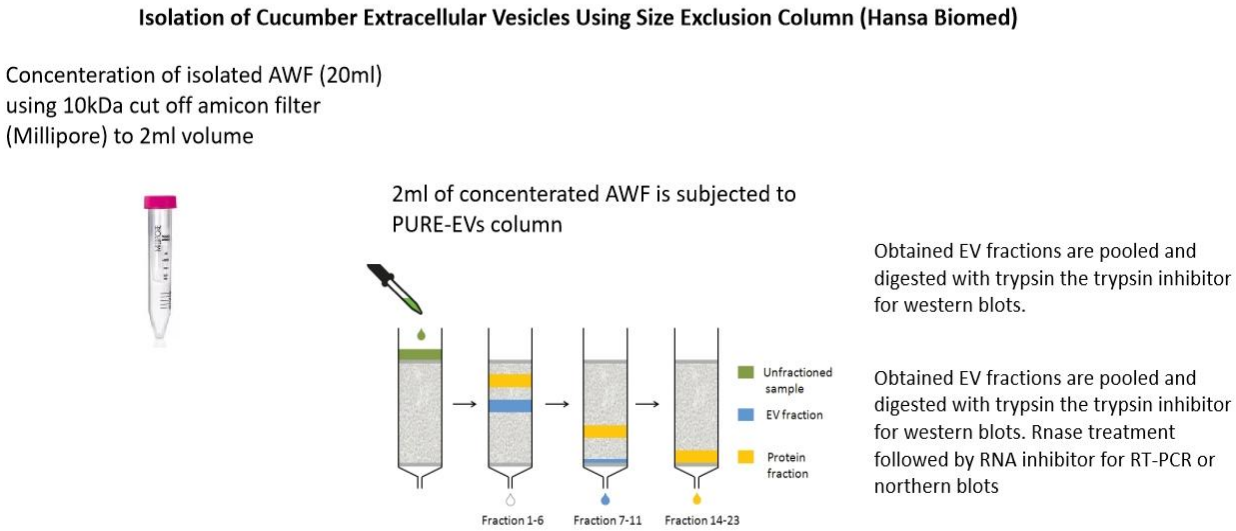

Fig. S2 showing the procedure followed for isolation of EVs from isolated AWF of cucumber

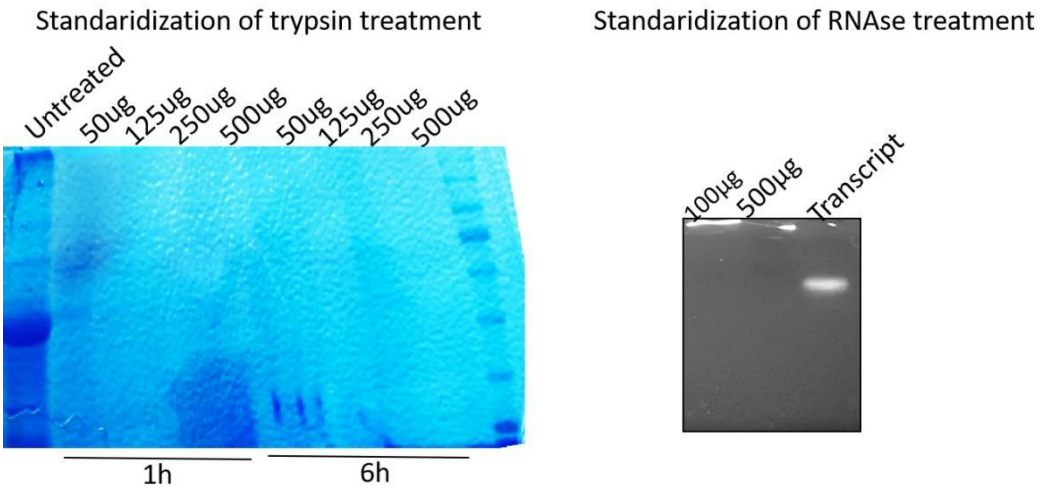

Fig. S3 and S4: Standardization of trypsin and RNase concentration for treatment of EVs with trypsin and RNase for protease protection assay.

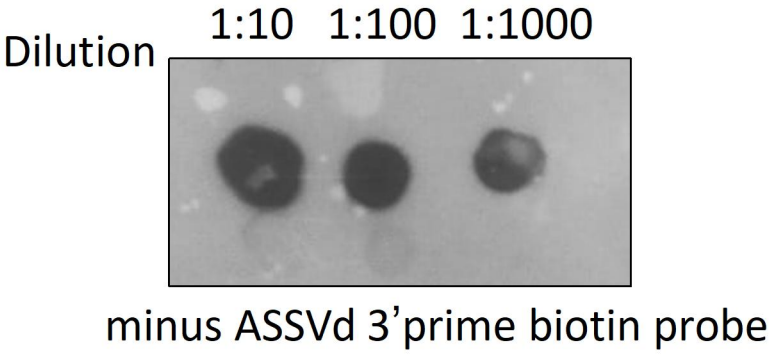

Fig. S5: Showing labeling of minus strand of ASSVd transcript with Biotin at its 3' end and its detection using anti anti-Streptavidin antibody.

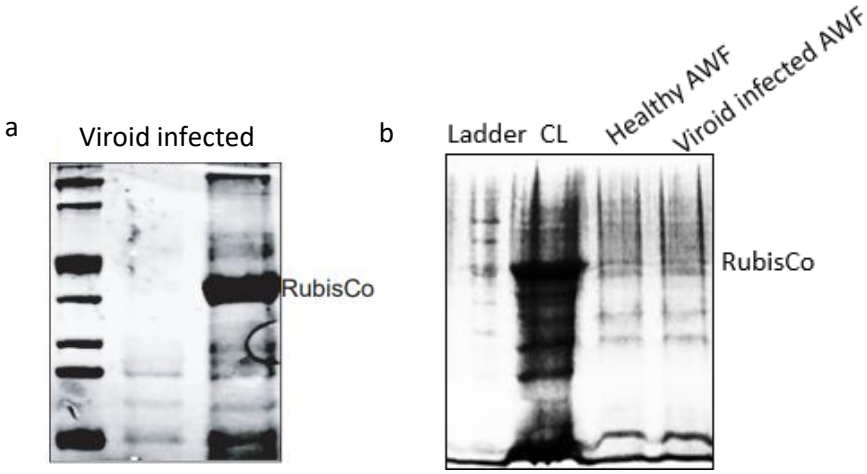

Fig S6 a and b) Coomassie staining of SDS PAGE with total protein extract isolated from AWF and whole cell lysate (CL). Absence of Rubisco protein at 55kDa in AWF fraction compared to CL indicate purity of AWF and absence of cytosolic contamination

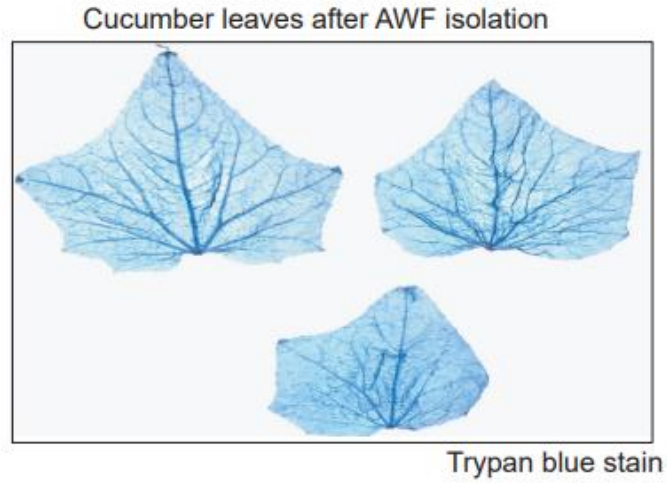

Fig. S7 Trypan blue staining of leaves used for AWF isolation. Absence of any cell damage as indicated by clear leaves suggest purity of isolated AWF free from cellular content.

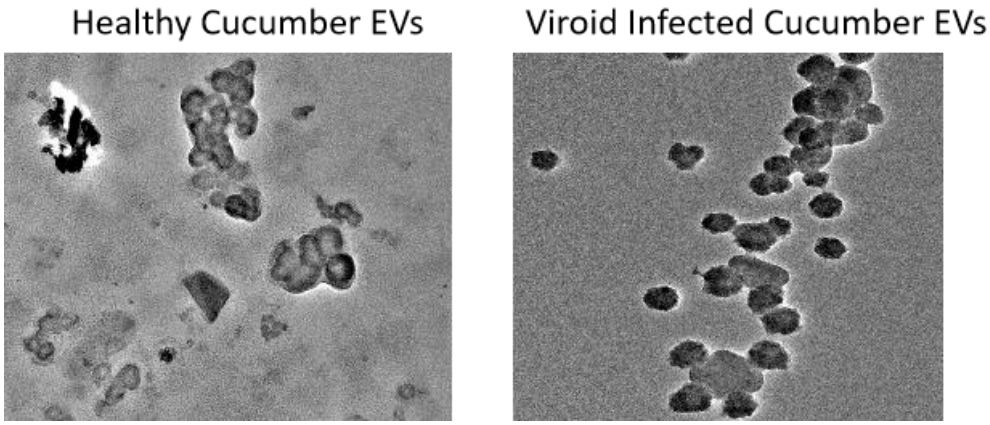

Fig. S8 Showing TEM images of EVs isolated from healthy cucumber apoplast and viroid infected cucumber apoplast

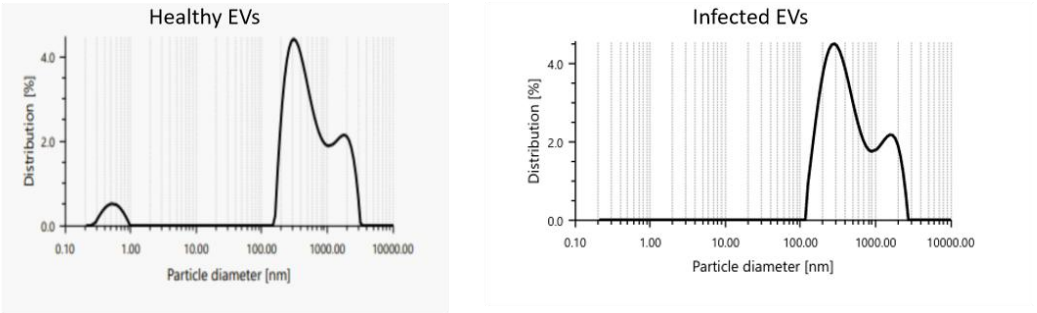

1007

1008 Fig. S9 Showing the diameter of particles in nanometre and particle distribution in percentage of
1009 EVs isolated from healthy cucumber apoplast and viroid infected cucumber apoplast.

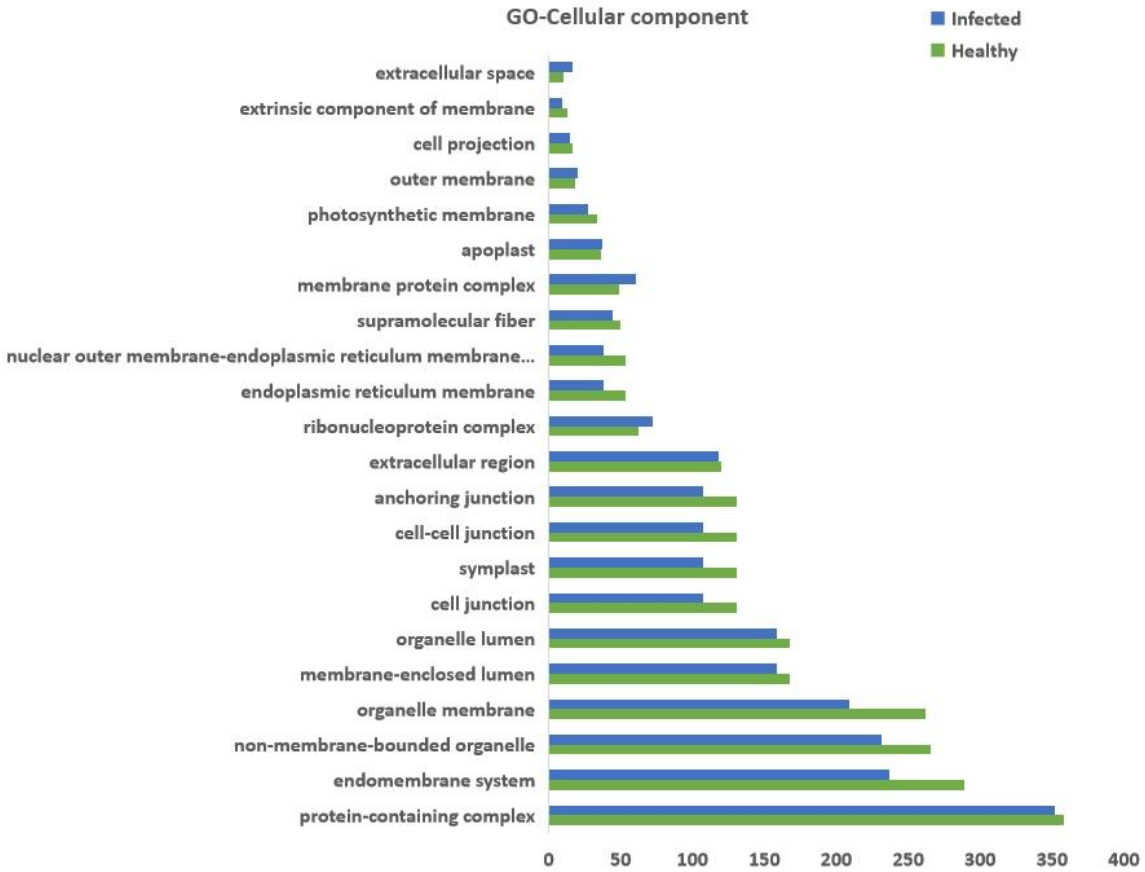

1010

1011

1012 Fig. S10 Bar showing classification of viroid infected and healthy EV proteins based on
1013 subcellular component

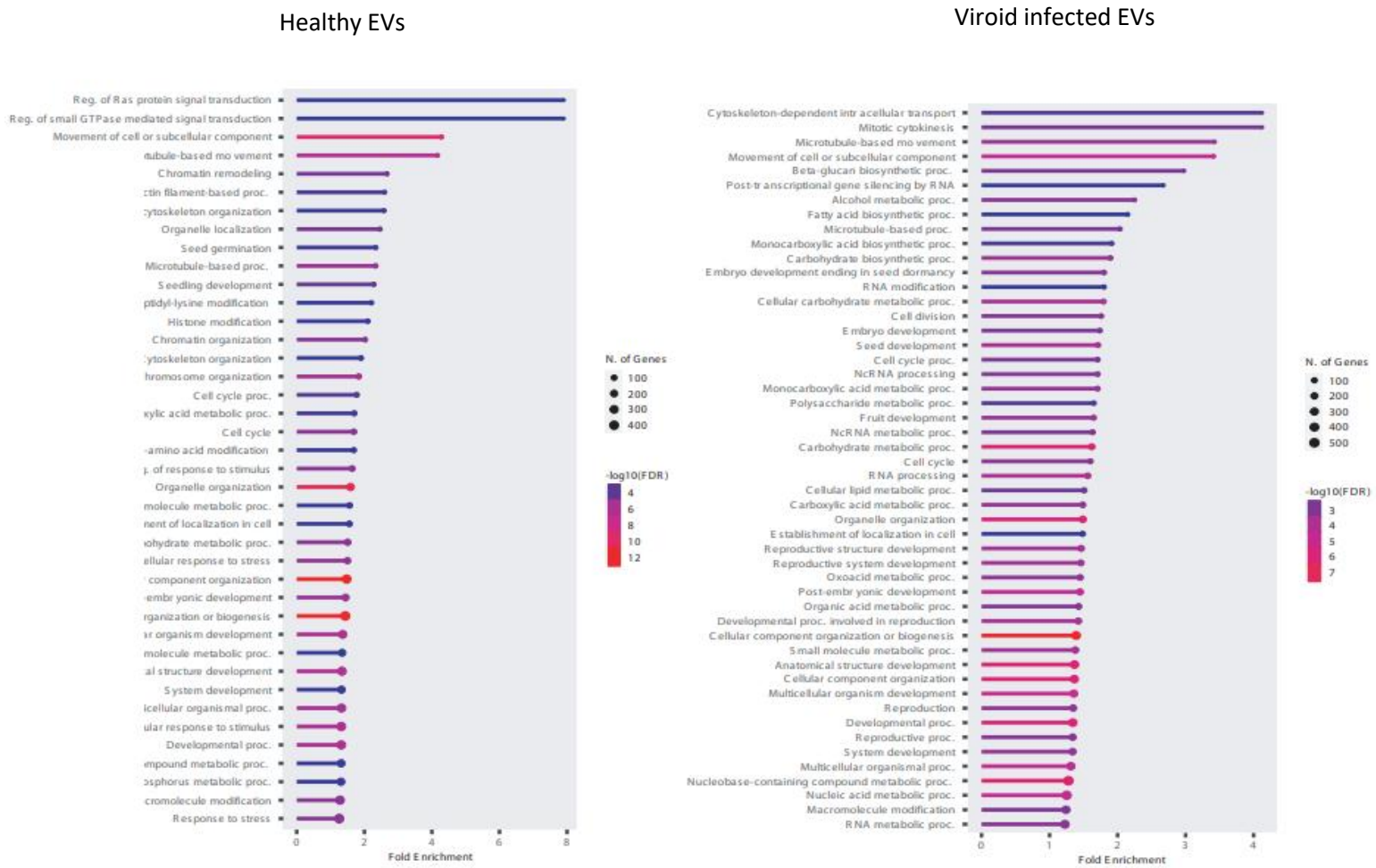

Fig. S11 Bar graph showing the classification of viroid infected and healthy EV proteins based on biological processes with notable enrichment of proteins related to non-coding RNA processes in viroid infected EVs compared to healthy EVs. (Each sample is pool of at least 50 biological replicates).

We tested whether Arabidopsis TET8 (AtTET8) antibodies would cross-react with cucumber Tet8 (CsTet8) protein and found that the Arabidopsis Tet8 (AT2G23810) ortholog in cucumber is Tet8/Lipoxygenase domain 3 (Csa1g287020) that shared 65.67% homology with AtTet8 (Fig. S7). Additionally, the 18 amino acids used to generate the peptide from the EC2 domain (Phytoab) were over 90% identical between the Arabidopsis and cucumber Tet8, suggesting that AtTet8 antibodies would cross-react with cucumber Tet8 (Fig. S8).

BLAST of Csa1G287020 vs. TAIR10
Match: AT2G23810.1 (AT2G23810.1 tetraspanin8)

HSP 1 Score: 397.5 bits (1020), Expect = 6.5e-111
Identity = 176/268 (65.67%), Postives = 216/268 (80.60%), Query Frame = 1

```
Query: 1   MVKLSNNLVGILNFITFLLSIPIIAGGIWLSRQGTSDCEKFLDTPVIVIGVFLLLVSLAG 60
           M + SNNLVGILNF+ FLLSIPI+AGGIWLS++G+++CE+FLD PVI +GVFL++V++AG
Sbjct: 1   MARCSNNLVGILNFLVFLLSIPILAGGIWLSQKGSTECERFLDKPVIALGVFLMVVAIAG 60

Query: 61  FIGACCRVRWLLWIYLFVMFLLILLLFVFTIFAFAVTNKGAGKVLSNRGYKEYRLGDYSN 120
            IG+CCRV WLLW+YLFVMFLLILL+F  T+FAF VTNKGAG+ +  +GYKEY+LGDYS
Sbjct: 61  LIGSCCRVTWLLWVYLFVMFLLILLVFCITVFAFVVTNKGAGEAIEGKGYKEYKLGDYST 120

Query: 121 WLQNRVRNNKDWNRIRSCLVDGKVCNEVSQKFVGETVEQFYLEHLSSIQSGCCKPADECK 180
           WLQ RV N K+WN+IRSCLV+ KVC+++  KFV   V  FY EHL+++QSGCCKP+DEC
Sbjct: 121 WLQKRVENGKNWNKIRSCLVESKVCSKLEAKFVNVPVNSFYKEHLTALQSGCCKPSDECG 180

Query: 181 FEYKGPIQWDKPANVSSFANPDCGLWDNDPQKLCFDCESCKGGVLDNLKRNWKKVAIINI 240
           FEY  P  W K     +  NPDC  WDN  +KLCFDC+SCK G+LDN+K  WKKVAI+NI
Sbjct: 181 FEYVNPTTWTK-NTTGTHTNPDCQTWDNAKEKLCFDCQSCKAGLLDNVKSAWKKVAIVNI 240

Query: 241 VILVFLIIVYSIGCCAFRNSKEENHYPR 269
           V LVFLIIVYS+GCCAFRN+K ++ Y R
Sbjct: 241 VFLVFLIIVYSVGCCAFRNNKRDDSYSR 267
```

Fig. S12 Sequence Homology between CsTET8 and AtTET8 showing 65.67% identity between the two proteins. The EC2 domain froM which the antibody of Phytoab AtTET8 is made is marked in red boxes

EC2 domain-97aa-235aa

```
                                        10        20        30        40        50        60        70        80        90       100       110       120       130       140
Sequence ID start end weight  ---------|---------|---------|---------|---------|---------|---------|---------|---------|---------|---------|---------|---------|---------|
1 _ATTET8      1 140      1 TNKGAGEAIEGKGYKEYKLGDYSTWLQKRVENGKNWNKIRSCLVESKVCSKLEAKFVNVPVNSFYKEHLTALQSGCCKPSDECGFEYVNPTTWTKNTT-GTHTNPDCQTWDNAKEKLCFDCQSCKAGLLDNVKSAWKKVA
1 _CSTET8      1 140      1 TNKGAGKVLSNRGYKEYRLGDYSNWLQNRVRNNKDWNRIRSCLVDGKVCNEVSQKFVGETVEQFYLEHLSSIQSGCCKPADECKFEYKGPIQWDKPANVSSFANPDCGLWDNDPQKLCFDCESCKGGVLDNLKRNWKKVA
2 Consensus             2.00 TNKGAGEAIENRGYKEYRLGDYSNWLQNRVRNNKNWNRIRSCLVDGKVCNELEQKFVNEPVNQFYKEHLTAIQSGCCKPADECGFEYKNPTQWDKPTNVGTHTNPDCGTWDNDPQKLCFDCQSCKGGLLDNLKRNWKKVA
```

Fig. S13: Multiple alignment between EC2 domain of CsTET8 and AtTET8 showing consensus sequences between the two proteins

To further confirm this cross-reactivity, we cloned CsTET8 (Csa_1g287020), the cucumber ortholog of AtTET8, into the pSITE2CA and HApBA plant binary vector with a GFP tag for visualization. These recombinant plasmid and were then transiently expressed in Nicotiana plants, and western blot analysis using anti-GFP, anti-TET8 and anti-AtTET8 antibodies confirmed that the AtTET8 antibodies effectively recognized CsTET8 (Fig. S14 and S15) at size of approximately 55kDa and 25kDa, respectively. Based on these findings, we proceeded to use the available AtTET8 antibodies in further experiments.

1050 **Generation of constructs**

1051 The CsTET8 gene (Csa1g287020) was amplified from cucumber plants using the RT-PCR
1052 method. In brief, RNA was extracted from healthy cucumber plants with RNAiso Plus. Reverse
1053 transcription was performed with the Verso cDNA synthesis kit (Thermo). PCR amplification
1054 was carried out using Phusion DNA polymerase (Thermo) with specific primers (CsTET8F/R)
1055 (Table S1). The PCR products were resolved on a 1.5% agarose gel, and the desired bands were
1056 excised and purified using the GeneJET Thermo kit. The purified fragments were then cloned
1057 into the pJET1.2 vector (Thermo) and transformed into TOP10 competent cells. The recombinant
1058 plasmid was sequenced, confirming 100% identity to CsTET8.

1059 The CsTET8 gene was further amplified using adaptor primers (CsTET8att F and CsTET8att R)
1060 and universal primers (Adaptor F/R) (Table S1). The amplified fragment was ligated into the
1061 PDONR207 vector using BP clonase (Invitrogen) and transformed into TOP10 competent cells.
1062 The transformed cells were plated on LA plates containing 100 mg/ml kanamycin. Recombinant
1063 plasmids were verified through colony PCR using the vector-specific primer (Nru R) and the
1064 gene-specific primer (CsTET8 F).

1065 Subsequently, the pDONR-CsTET8 clone was sub cloned into the pSITE2CA vector and the
1066 HA-pBA vector (Chakrabarty et al., 2007) for expression under the CaMV35S promoter, with
1067 N-terminal GFP and HA tags, respectively, using the LR clonase enzyme (Thermo Scientific,
1068 USA). The ligated products were transformed into LA plates containing 50 mg/ml spectinomycin.
1069 Recombinant clones were screened by colony PCR with the CaMV35S forward primer and
1070 CsTET8R primer. The GFP-TET8 and HA-TET8 constructs were then transformed into the
1071 Agrobacteriun strain GV3101 using chemical transformation and used for transient expression
1072 analysis in *Nicotiana benthamiana* plants, as described by Walia et al. (2020).

1073

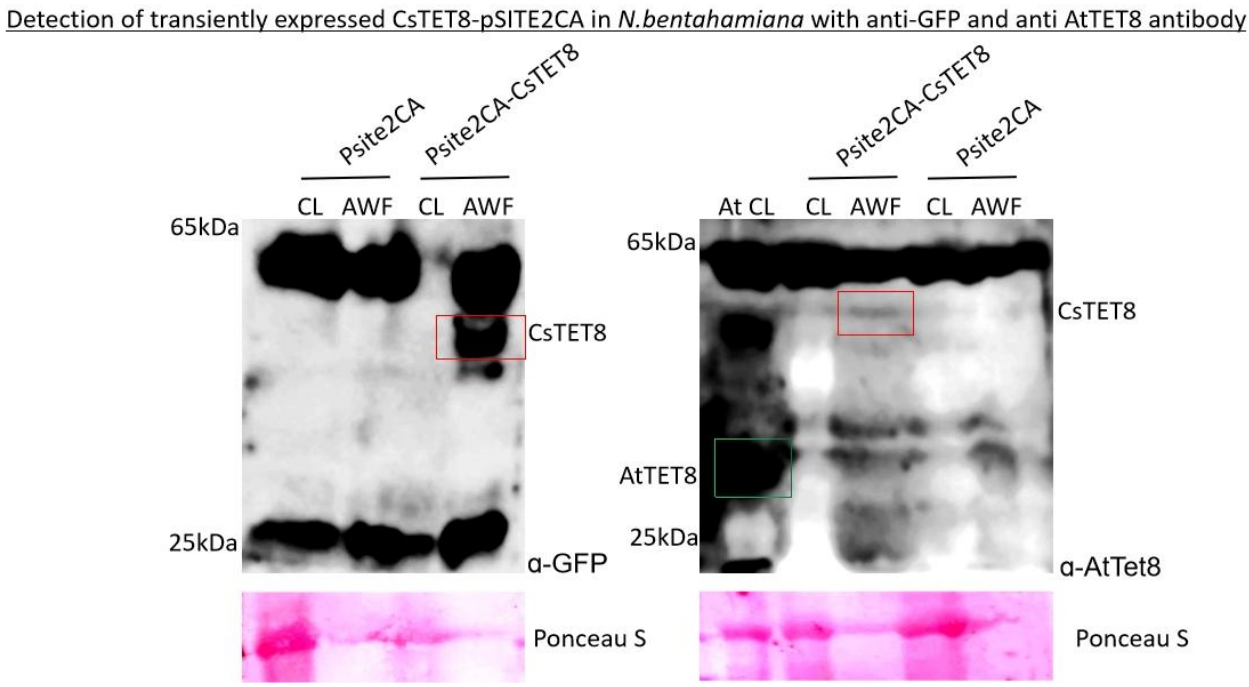

Fig. S14: a and b: western blot of *N. benthamiana* cell lysate (CL) and AWF showing transient expression of CsTET8-pSITE2CA in and empty vector (pSITE2CA) with 25kDa band corresponding to the size of only GFP and app. 55kDa size of CsTET8+GFP detected with (a) anti-GFP antibody. (b) AtTE8 antibody. The band corresponding to the size of CsTET8+GFP is detected in AWF and marked in the box. The arabidopsis TET8 band detected with AtTET8 antibody at 30kDa as positive control is marked in the green box (Fig.S9b)

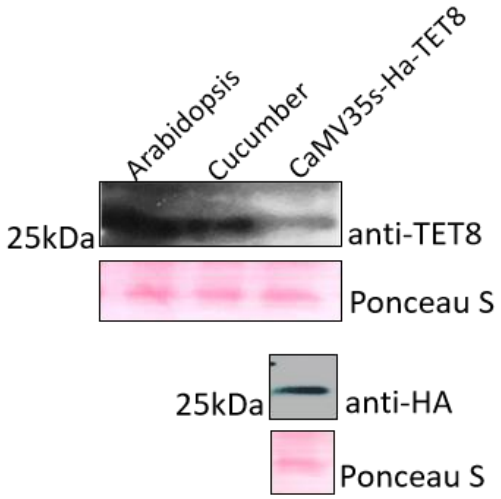

Fig. S15: western blot of *N. benthamiana* cell lysate (CL) showing transient expression of HA-CsTET8 and arabidopsis and cucumber cell lysate as control showing 30kDa band corresponding to the size of TET8 with anti-TET8 antibody and anti-HA antibody.

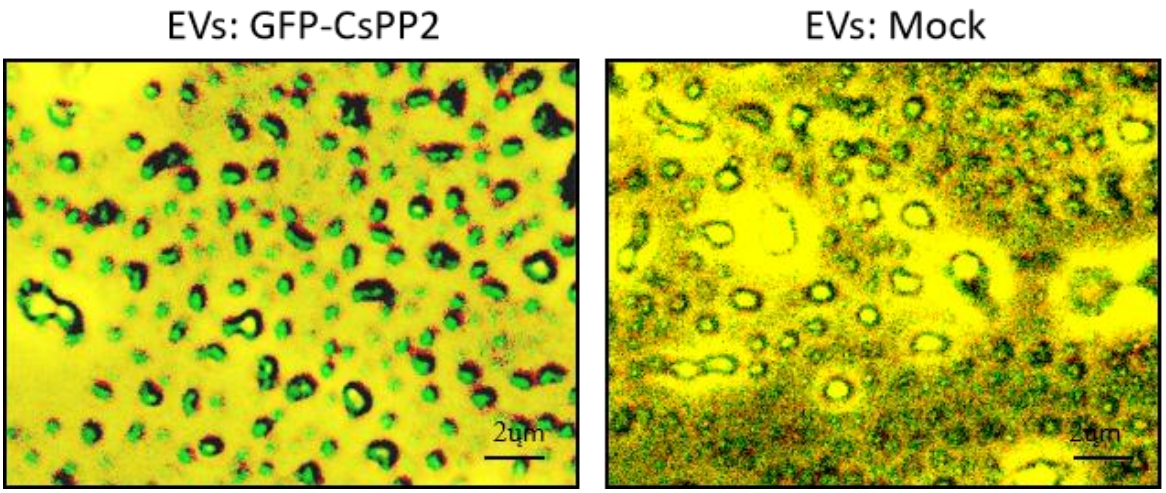

Fig. S16 Image showing EVs from GFP-CsPP2 expressing *N. benthamiana* and mock plants as visualized under fluorescence microscope using GFP Filter

The subcellular localization of CsTET8 was monitored by transiently expressing the CsTET8-pSITE2CA in *N. benthamiana* which revealed the cytoplasmic and plasma membranous localization of CsTET8.

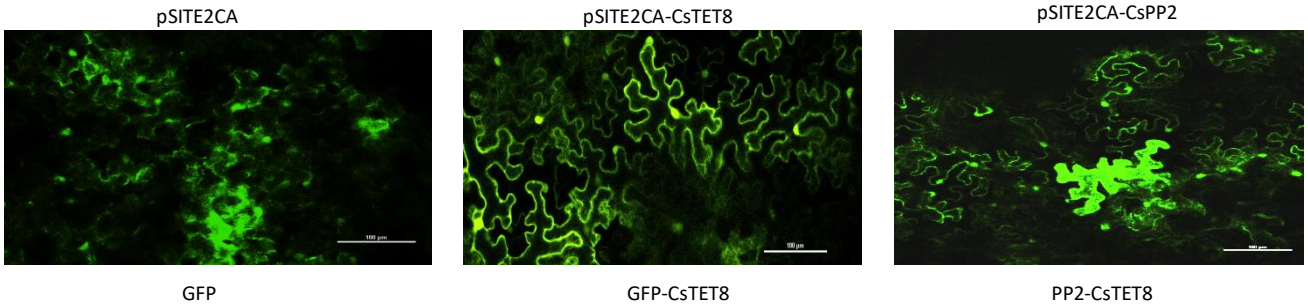

Fig. S17: Localization of GFP-CsTET8 and GFP-CsPP2 in *N. benthamiana*. Speckles are observed on plasma membrane for both CsTET8 and CsPP2 hinting towards its association with membranous bodies.

VIROIDS	TGTG	CCGGUCG	CCGGTG	CTGGGG	CGGGAG	UCCC	CUCC	CCCU	UGUG	GGUG	TAATCCCA	ACCCTGCCGCCTGGACTCCGCCTGT
Citrus viroid												
Citrus exocortis viroid												
Apple scar skin viroid												
Hop stunt viroid												
Potato spindle tuber viroid												
Avocado sunblotch viroid												
Iresine stunt viroid												
Columnea latent viroid												
Grapevine yellow speckle viroid												
Hopstunt viroid												
Tomato apical stunt viroid												✓
Citrus bent leaf viroid												
Citrus stunt viroid												
Coconut tinjanga viroid												
Citrus dwarf viroid												
Tomato chlorotic dwarf viroid												
Citrus chaxia viroid												
Tomato macho viroid												
Apple chlorotic viroid												
Permission viroid												
Dahlia latent viroid												
Pear blister canker viroid												
Apple hammerhead viroid												
Apple dimple fruit viroid												
Australian grapevine viroid												
Pepperchat fruit Viroid												
Japanese citrus viroid												
Coconut cadang cadang viroid												
Citrus latent viroid												
Citrus Barking viroid												

Fig. S18: EXOmotifs observed in various viroids

Predicted localizations: Cytoplasm
Predicted membrane association: Transmembrane
Predicted signals:

Localization	Cytoplasm	Nucleus	Extracellular	Cell membrane	Mitochondrion	Plastid	Endoplasmic reticulum	Lysosome/Vacuole	Golgi apparatus	Peroxisome
Probability	0.6230	0.1612	0.0481	0.4090	0.1147	0.0078	0.1282	0.2419	0.2050	0.0001

Membrane association	Peripheral	Transmembrane	Lipid anchor	Soluble
Probability	0.3120	0.6770	0.4410	0.4090

Fig. S19 Showing the presence of transmemberane domain in the CsPP2 as analyzed using DeepLoC 2.1 tool (DeepLoc 2.1 - DTU Health Tech - Bioinformatic Services)

Primer name	Sequence
ASSVdICC	GTCGACGAAGGCCGGTGAGAA
ASSVd ICH	GTCGACGACGACAGGTGAGTT
CsTET8 f	ATGGTCAAACTCAGCAATAATCTC
CsTET8 r	TCATTTCCATCTAGGATAATG
CsTET8 att F	AAAAAGCAGGCTCAATGGTCAAACTCAGCAATAATC
SCsTET8 att R	AGAAAGCTGGGTATCATTTCCATCTAGGATAATG
Adaptor F	GGG GAC AAG TTT GTA CAA AAA AGC AGG CT
Adaptor R	GGG GAC CAC TTT GTA CAA GAA AGC TGG GT
CaMV35S	GACTCACTATAGGGAGAG
Nru R	ACGGAAACAGCTATGAC
CsPP2-HIS F BamH1	GAGGATCCATGGTTTGCATAGAGACAGAA
CsPP2-HIS R Xho1	GACTCGAGTTTAGCATCCGCAACTGGATT
CsPP2 att F	AAAAAGCAGGCTCAAATGGTTTGCATAGAGACAGAA
CsPP2 att R	AGAAAGCTGGGTATAAAAAGCAGGCTCAA

FP1	AGTAATACGACTCACTATAGGGGGGAAACACCTATTGTGTT
RP4	GGTAAACACCGTGCGGTTC

1114

1115

1116 **Table S1:** Primers used during the study

1117

1118

1119

1120